AD A138 722 THEORETICAL INVESTIGATION OF THREE-DIMENSIONAL SHOCK WAVE-TURBULENT BOUND..(U) RUTGERS - THE STATE UNIV NEW BRUNSWICK N J DEPT OF MECHANICAL.. D D KNIGHT DEC 83 1/1

UNCLASSIFIED RU-TR-160-MAE-F AFOSR-TR-84-0113 F/G 20/4 NL

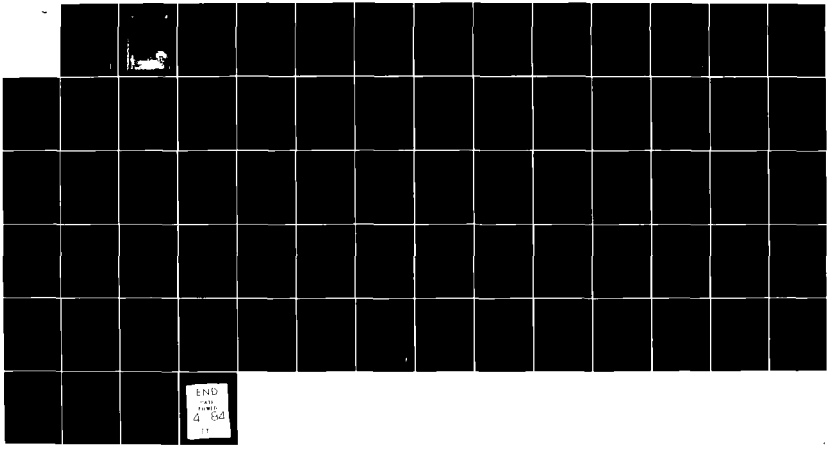

END
DATE FILMED
4 84
DTIC

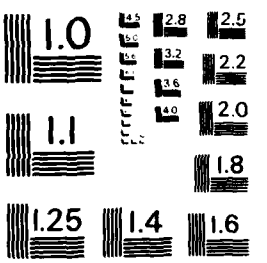

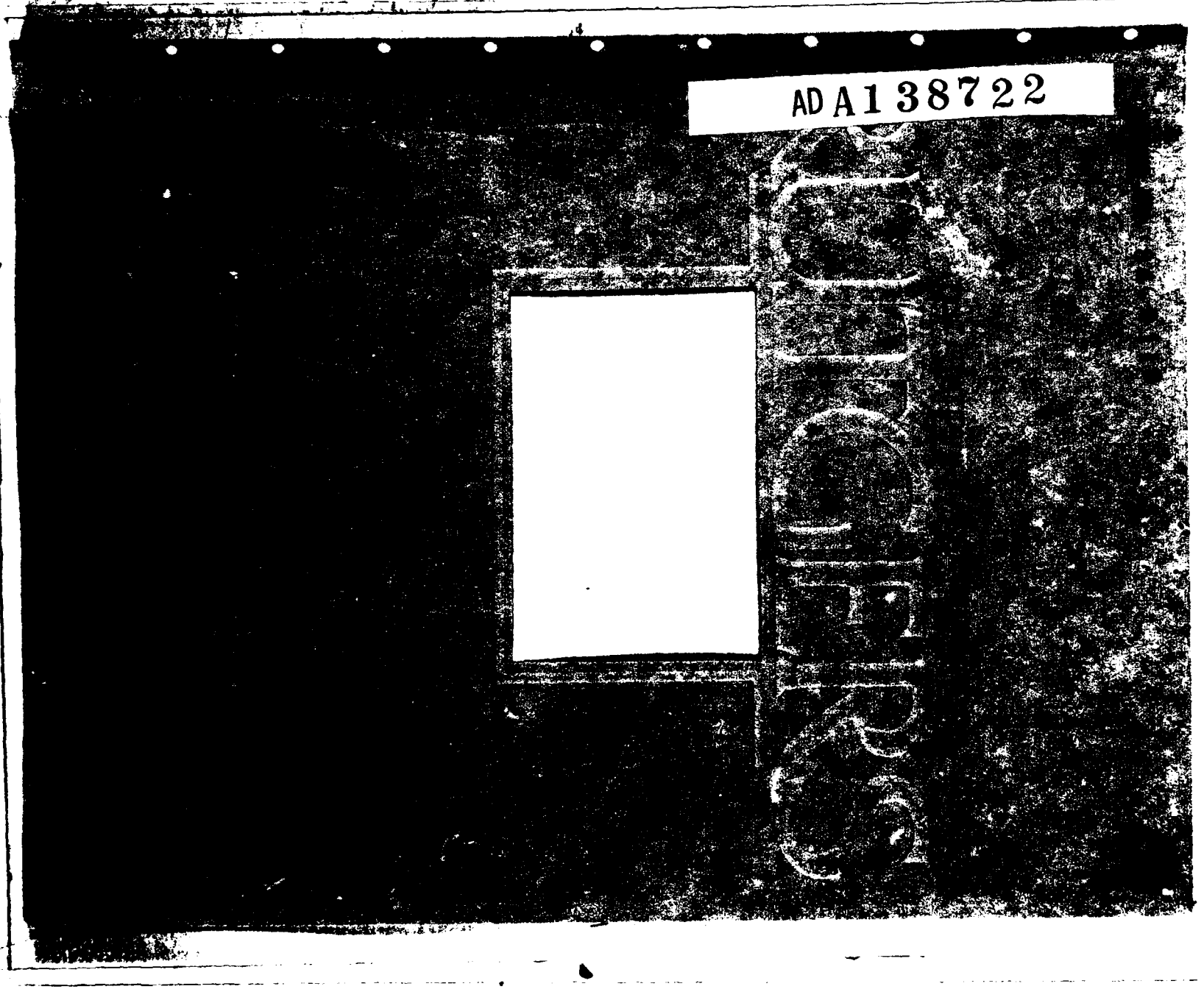
AD A138722

2

Department of Mechanical and Aerospace Engineering
Rutgers University
New Brunswick, New Jersey 08903

Report RU-TR-160-MAE-F

THEORETICAL INVESTIGATION OF THREE-DIMENSIONAL SHOCK WAVE-TURBULENT BOUNDARY LAYER INTERACTIONS

Part II

Doyle D. Knight

~~Interim~~ Report for Period 1 October 1982 to 30 September 1983

Air Force Office of Scientific Research
Building 410
Bolling AFB
Washington, DC 20332

December 1983

UNCLASSIFIED

SECURITY CLASSIFICATION OF THIS PAGE (When Data Entered)

REPORT DOCUMENTATION PAGE		READ INSTRUCTIONS BEFORE COMPLETING FORM
1. REPORT NUMBER AFOSR-TR- 84-0113	2. GOVT ACCESSION NO. AD A135422	3. RECIPIENT'S CATALOG NUMBER
4. TITLE (and Subtitle) THEORETICAL INVESTIGATION OF THREE-DIMENSIONAL SHOCK WAVE-TURBULENT BOUNDARY LAYER INTERACTIONS - Part II		5. TYPE OF REPORT & PERIOD COVERED Annual 1 Oct. 1982 to 30 Sept. 1983 6. PERFORMING ORG. REPORT NUMBER
7. AUTHOR(s) Prof. Doyle D. Knight		8. CONTRACT OR GRANT NUMBER(s) AFOSR-82-0040
9. PERFORMING ORGANIZATION NAME AND ADDRESS Dept. of Mechanical & Aerospace Engineering Rutgers University New Brunswick, N.J. 08903		10. PROGRAM ELEMENT, PROJECT, TASK AREA & WORK UNIT NUMBERS 2307/A1 61102F
11. CONTROLLING OFFICE NAME AND ADDRESS Air Force Office of Scientific Research /NA Building 410 Bolling AFB, DC 20332		12. REPORT DATE December 1983 13. NUMBER OF PAGES 69
14. MONITORING AGENCY NAME & ADDRESS(if different from Controlling Office)		15. SECURITY CLASS. (of this report) UNCLASSIFIED 15a. DECLASSIFICATION/DOWNGRADING SCHEDULE

16. DISTRIBUTION STATEMENT (of this Report)

Approved for Public Release; Distribution Unlimited

17. DISTRIBUTION STATEMENT (of the abstract entered in Block 20, if different from Report)

18. SUPPLEMENTARY NOTES

19. KEY WORDS (Continue on reverse side if necessary and identify by block number)

High Speed Flows; Viscous-Inviscid Interactions; Shock-Boundary Layer Interactions; Computational Fluid Dynamics; Navier-Stokes Equations; Turbulence

20. ABSTRACT (Continue on reverse side if necessary and identify by block number)

The focus of the research effort is the understanding of three-dimensional shock wave-turbulent boundary layer interactions. The approach uses the full mean compressible Navier-Stokes equations with turbulence incorporated through the algebraic turbulent eddy viscosity model of Baldwin and Lomax. During the present year of the research effort, the three-dimensional shock boundary layer interaction generated by a 10 deg sharp fin has been computed at Mach 3 for a Reynolds number $Re_\infty = 2.8 \times 10^7$. These results, together with previous

DD FORM 1 JAN 73 1473 EDITION OF 1 NOV 65 IS OBSOLETE

280000

UNCLASSIFIED

SECURITY CLASSIFICATION OF THIS PAGE (When Data Entered)

20. ABSTRACT

Reynolds number = 930000

computations of the same configuration at $Re_{\delta_\infty} = 9.3 \times 10^5$, are compared with experimental data for pitot pressure and yaw angle. The agreement with the experimental data is good, and the theory accurately predicts the recovery of the boundary layer downstream of the interaction at $Re_{\delta_\infty} = 2.8 \times 10^5$. The computed flowfield is employed to analyze the structure of the 3-D interaction through contour plots of flow variables. Also, during the present year, the investigation of the 2-D turbulent supersonic compression corner at Mach 3 was completed. The relaxation modification to the Baldwin-Lomax model was found to yield reasonably accurate predictions of the upstream propagation of the surface for the Re_{δ_∞} range investigated. An additional computation at Mach 2 was performed, and the results were in general in agreement with the previous conclusions.

Reynolds number

Reynolds number =
29000

PREFACE

This report presents the research accomplishments for the second year (1 October 1982 to 30 September 1983) of the research investigation entitled "Theoretical Investigation of Three-Dimensional Shock-Wave Turbulent Boundary Layer Interactions". The research has benefited from the assistance of several individuals, including Dr. James Wilson (Air Force Office of Scientific Research), and Drs. James Keller and Jerry South (NASA Langley Research Center). The important and helpful interactions with Professors Seymour Bogdonoff, Dave Dolling, Gary Settles, and Lex Smits are also acknowledged.

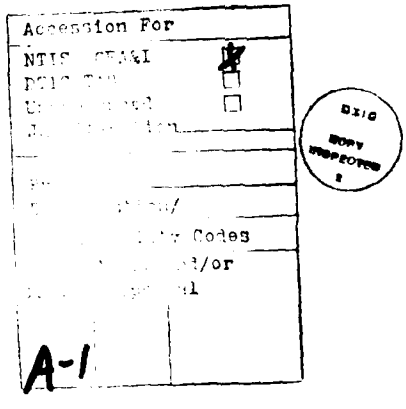

TABLE OF CONTENTS

I. Introduction. 8

II. Status of Research for the Second Year and Schedule of Research for the Remainder of the Third Year 10

A. 2-D Supersonic Compression Ramp Studies. 10
B. 3-D Supersonic Sharp Fin Studies 18
C. Tables 32
D. Figures. 37

III. Publications and Scientific Interactions. 60

A. Written Publications 60
B. Interaction with Research Group at Princeton Gas Dynamics Laboratory. 60
C. Spoken Papers Presented at Technical Meetings. . 63
D. Seminars 64

IV. List of Personnel and Degrees Awarded 65

V. References. 66

LIST OF ILLUSTRATIONS

Fig. 1 Geometry of 2-D supersonic compression ramp 38

Fig. 2 Surface pressure for α = 20 deg, Re_{δ_∞} = 0.76 x 10^6 at M_∞ = 2.9. . . 39

Fig. 3 Surface pressure for α = 20 deg, Re_{δ_∞} = 3.4 x 10^6 at M_∞ = 2.9. . . 39

Fig. 4 Surface pressure for α = 20 deg, Re_{δ_∞} = 5.6 x 10^6 at M_∞ = 2.9. . . 40

Fig. 5 Surface pressure for α = 20 deg, Re_{δ_∞} = 7.7 x 10^6 at M_∞ = 2.9. . . 40

Fig. 6a Definition of Interaction Geometric Distances 41

Fig. 6b Effect of Re_{δ_∞} on Interaction Lengths for α = 20 deg at M_∞ = 2.9 . 42

Fig. 7 Surface pressure for α = 16 deg, Re_{δ_∞} = 0.25 x 10^6 at M_∞ = 1.96. . 43

Fig. 8 Geometry of 3-D Supersonic Sharp Fin 44

Fig. 9 Experimental Data Stations of Oskam. 45

Fig. 10 Experimental Data Stations of McClure. 45

Fig. 11a Pitot pressure at x_s/δ_0 = -8.98 for Case 1 46

Fig. 11b Pitot pressure at x_s/δ_0 = -5.84 for Case 2 46

Fig. 12a Pitot pressure at x_s/δ_0 = -1.71 for Case 1 47

Fig. 12b Pitot pressure at x_s/δ_0 = -1.76 for Case 2 47

Fig. 13a Pitot pressure at x_s/δ_0 = -0.63 for Case 1 48

Fig. 13b Pitot pressure at x_s/δ_0 = -0.78 for Case 2 48

Fig. 14a Pitot pressure at x_s/δ_0 = 1.0 for Case 1 49

Fig. 14b Pitot pressure at x_s/δ_0 = 1.27 for Case 2. 49

Fig. 15a Pitot pressure at x_s/δ_0 = 4.23 for Case 1. 50

Fig. 15b Pitot pressure at x_s/δ_0 = 3.4 for Case 2 50

Fig. 16 Pitot pressure at x_s/δ_0 = 14.2 for Case 1. 51

Fig. 17 Pitot pressure at x_s/δ_0 = 20.7 for Case 2. 51

Fig. 18a Yaw angle at x_s/δ_0 = -8.98 for Case 1. 52

Fig. 18b Yaw angle at x_s/δ_0 = -5.84 for Case 2. 52

Fig. 19a Yaw angle at x_s/δ_0 = -1.71 for Case 1. 53

Fig. 19b Yaw angle at x_s/δ_0 = -1.76 for Case 2. 53

Fig. 20a Yaw angle at x_s/δ_0 = -0.63 for Case 1. 54

Fig. 20b Yaw angle at x_s/δ_0 = -0.78 for Case 2. 54

Fig. 21a Yaw angle at x_s/δ_0 = 1.0 for Case 1. 55

Fig. 21b Yaw angle at x_s/δ_0 = 1.27 for Case 2 55

Fig. 22a Yaw angle at x_s/δ_0 = 4.23 for Case 1 56

Fig. 22b Yaw angle at x_s/δ_0 = 3.4 for Case 2. 56

Fig. 23 Yaw angle at x_s/δ_0 = 14.2 for Case 1 57

Fig. 24 Yaw angle at x_s/δ_0 = 20.7 for Case 2 57

LIST OF TABLES

Table 1 Summary of Experimental Data for 2-D Supersonic Compression Ramp at Mach 3 32

Table 2 Summary of Computations for 2-D Supersonic Compression Ramp at Mach 3 33

Table 3 Summary of Experimental Data of Oskam and McClure for 3-D Sharp Fin at Selected α_g 34

Table 4 Summary of Computations for 3-D Sharp Fin. 35

Table 5 Flow Conditions for Experiments of McClure for 3-D Sharp Fin . . 35

Table 6 Flow Conditions for Computations of 3-D Sharp Fin at α_g = 10 deg. 36

I. Introduction

The understanding of two- and three-dimensional shock wave-turbulent boundary layer interactions (denoted as "2-D" or "3-D turbulent interactions") continues to remain an important area of research effort in fluid dynamics. In aerodynamics, important examples of 3-D turbulent interactions include transonic airfoils, supersonic inlets, nozzles, and deflected control surfaces and wing-body junctures at transonic and supersonic speeds [1,2]*. In other applications in fluid dynamics (e.g., gas dynamic lasers [3]), 3-D turbulent interactions are important as well.

The goals of the present research program, as outlined in the original proposal [4], remain unchanged. For convenience, they are listed below:

1. To determine the accuracy of theoretical predictions of 3-D shock wave-turbulent boundary layer interactions by numerical solution of the three-dimensional compressible Navier-Stokes equations with a turbulent eddy viscosity model.
2. To investigate the physical structure of 3-D shock wave-turbulent boundary layer interactions in simplified geometries (e.g., swept compression corner, swept fin and sharp fin configurations) through a close cooperative effort consisting of numerical computation by the present investigator and experimental studies by the Princeton Gas Dynamics Laboratory.
3. To evaluate the hypothesized physical structures of 3-D turbulent interactions at a variety of conditions outside the range of the experiments (e.g., different Mach numbers and geometries).

*References are listed in Section V.

The research effort during the second year has focused on two major flow configurations. First, the extensive study of the two-dimensional turbulent compression corner, begun during the first year, has been completed. Second, the three-dimensional turbulent interaction generated by a sharp fin has been examined at two different Reynolds numbers. The results are presented in detail in the following section.

II. Status of the Research for the Second Year and Schedule of Research for the Remainder of the Third Year

A. Calculation of Two-Dimensional Supersonic Compression Ramp Flows

1. Objectives

The objectives of the 2-D supersonic turbulent compression ramp studies are twofold, namely:

a. To examine the accuracy of the Baldwin-Lomax [5] algebraic turbulent eddy viscosity model for the computation of 2-D turbulent interactions.

The algebraic turbulent eddy viscosity model of Baldwin and Lomas [5] was adopted for the 3-D turbulent interaction research [4]. Although the mode' has been employed for a variety of 3-D flowfield calculations [6-9], it had not been critically examined for 2-D turbulent interactions. Consequently, it was deemed necessary to undertake a concurrent evaluation of the model for 2-D turbulent interactions.

b. To develop sensible modifications, within the inherent limitations of the algebraic eddy viscosity concept, to improve the flowfield predictions.

Based upon previous experience [10,11] in the prediction of 2-D turbulent interactions using various algebraic eddy viscosity models, it was anticipated that improvements in the flowfield prediction would be sought through simple modifications to the turbulence model.

2. Experimental Configuration

The flow configuration for the 2-D turbulent compression ramp is

displayed in Fig. 1. A supersonic equilibrium turbulent boundary layer is deflected by an angle α, generating a shock-turbulent boundary layer interaction in the vicinity of the corner. The experimental data, obtained by Settles and his colleagues at the Princeton Gas Dynamics Laboratory [12-14], may be categorized into two major areas as indicated in Table 1, namely, 1) flowfield profiles for four corner angles (α = 8, 16, 20 and 24 deg) at a fixed Reynolds number $Re_{\delta_\infty} = 1.6 \times 10^6$ (where Re_{δ_∞} is the Reynolds number based on the boundary layer thickness δ_∞ upstream of the interaction), and 2) surface pressures for a fixed ramp angle α = 20 deg for a range of Reynolds numbers $Re_{\delta_\infty} = 0.76 \times 10^6$ to 7.7×10^6. The first category includes measurements of a) surface pressure, b) skin friction, and c) velocity, Mach number and static pressure profiles at nine streamwise stations for each ramp angle. The second category includes surface pressure, and separation and reattachment locations.

3. Method of Solution

The governing equations are the full mean compressible Navier-Stokes equations in two dimensions using mass-averaged variables [15], strong conservation form [9], and general curvilinear coordinates. The fluid is assumed to be a perfect gas, and the molecular viscosity is specified by Sutherland's law. The molecular and turbulent Prandtl numbers are 0.72 (air) and 0.9, respectively.

The algebraic turbulent eddy viscosity model of Baldwin and Lomax [5] is utilized. A total of three different versions of the model were employed as follows:

a. Unmodified Baldwin-Lomax Model

This is the original model proposed by Baldwin and Lomax [5].

b. Modified Baldwin-Lomax Model

This version incorporates two modifications to the original model, namely, 1) utilization of the local value of the shear stress in the Van Driest damping factor, and 2) modification of the method for determining the length and velocity scales in the outer portion of the boundary layer. These modifications are discussed in Refs. 16 and 17. The purpose for the first modification was to improve the prediction of the boundary layer in the vicinity of reattachment. The objective of the second modification was to reduce unphysical oscillations in the computed turbulent length scale in the vicinity of the corner.

c. Baldwin-Lomax Model with Relaxation

This version incorporates the turbulence relaxation model of Shang and Hankey [11], originally proposed for the Cebeci-Smith [18] algebraic eddy viscosity model, into the modified Baldwin-Lomax model. The purpose for this modification is to incorporate, in a simple fashion, the observation that the turbulence structure responds slowly to rapid changes in the mean flow [19,20].

The boundary conditions for the numerical computations may be categorized into four major areas. First, on the upstream boundary, the flow variables are specified from a flat plate boundary layer solution whose momentum thickness is equal to the experimental value. Second, on the solid boundary, the velocity vector is set to zero, the wall temperature is specified from the experiment, and the normal gradient of the pressure is obtained from the normal component of the momentum equation evaluated at the wall. Third, on the upper boundary, a no-reflection condition is imposed [16]. Fourth, on the downstream boundary, the zero outwards normal gradient condition is applied to the flow.

The numerical algorithm used to solve the Navier-Stokes equations is the

second-order accurate implicit approximate factorization method of Beam and Warming [21]. The upstream boundary layer profile (Fig. 1) was obtained by computing a developing flat plate turbulent boundary layer to the location at which the computed and experimental upstream momentum thickness were identical. The computed and experimental upstream velocity profiles [16,17] showed close agreement with the Law of the Wall and Wake [22].

A boundary-fitted numerical grid, generated by the method of Visbal and Knight [23], was employed for each computation. The grid points were distributed in a highly non-uniform manner, with refined spacing in the direction normal to the boundary and in the streamwise direction within the interaction region. The average number of grid points for each calculation was approximately 1900. The normal mesh spacing near the wall was chosen to accurately resolve the viscous sublayer, and typically 25 to 30 grid points were contained within the boundary layer at all stations. The minimum streamwise grid spacing varied from 0.027 δ_∞ to 0.077 δ_∞ depending on the case. Full details of the mesh distribution are provided by Ref. 17.

A total of seventeen (17) cases have been computed over the combined first and second year of the research program. The specific cases are listed in Table 2. It is noted that comparison has been made with <u>all</u> of the experimental data of Settles et al. [14], although only a limited number of results are presented herein for brevity.

4. Brief Review of Results for First Year - (1 Oct. 1981 - 30 Sept. 1982)

During the first year of the research effort, the principal focus of the 2-D interaction study was the computation of the compression ramp flows at fixed Reynolds number $Re_{\delta_\infty} = 1.6 \times 10^6$. Most of the cases listed in this category in Table 2 were completed during this period, and the results have been discussed in the Annual Scientific Report for the first year [24]. The

overall conclusions of the first and second years' study are included in Section II.A.6 below.

5. Summary of Results for Second Year - (1 Oct. 1982 - 30 Sept. 1983)

a. *Compression Ramp at Mach 3*

The principal focus of the second years' effort for the 2-D compression ramp was the calculation of the four different Reynolds number configurations at α = 20 deg. All of the computations utilized the Baldwin-Lomax model with the relaxation modification. The relaxation length scale was taken to be equal to δ_∞, as determined by previous examination of the α = 24 deg, $Re_{\delta_\infty} = 1.6 \times 10^6$ case.

The calculated and experimental surface pressure distributions are shown in Figs. 2 through 5 for Reynolds numbers Re_{δ_∞} from 0.76×10^6 to 7.7×10^6. In general, the extent of the upstream propagation of the surface pressure is predicted with reasonable accuracy. All of the computed profiles display a plateau which is associated with the separation region. In the $Re_{\delta_\infty} = 0.76 \times 10^6$ case the computed profile is in close agreement with the experiment, while at the higher Reynolds numbers the calculated plateau is somewhat more pronounced than in the experiment.

In Fig. 6a, definitions are shown for the upstream pressure propagation length ΔX_p, the separation length ΔX_s, and the overall separation-to-reattachment length L_s. The computed and experimental results for these quantities are displayed in Fig. 6b. In regards to the upstream propagation length ΔX_p, the computed results are in reasonable agreement with experiment, with a maximum difference of 20% at $Re_{\delta_\infty} = 0.76 \times 10^6$. Although the computed ΔX_p displays the general dependence on Reynolds number (with excellent agreement at higher Reynolds numbers), it is evident that the discrepancy between calculated and measured ΔX_p increases with decreasing Re_{δ_∞}. This indicates that the value of

the relaxation length necessary for close agreement with experimental at the lower Reynolds numbers is greater than the value employed (i.e., δ_∞). The upstream separation distance ΔX_s is overestimated by approximately 50% to 60%. However, the computations predict qualitatively the observed decrease of ΔX_s with increasing Reynolds number. These features are in agreement with the results of Horstman et al. [10] for the same configuration using the Cebeci-Smith model [18] with a relaxation length equal to δ_∞. The overall separation-to-reattachment length L_s is significantly overpredicted, due to the inability of the turbulence model to simulate the rapid increase in turbulent mixing in the vicinity of reattachment [25,26].

b. Compression Ramp at Mach 2

A single computation of a supersonic turbulent compression ramp at Mach 1.96 was performed during the second year in order to further evaluate the Baldwin-Lomax model with the relaxation modification. The specific case was α = 16 deg and $Re_{\delta_\infty} = 0.25 \times 10^6$. This represents a separated ramp flow according to the experiments performed at the Princeton Gas Dynamics Laboratory. A relaxation length equal to the upstream boundary layer thickness δ_∞ was employed, in agreement with the previous studies at $M_\infty = 3$ for $0.76 \times 10^6 \leq Re_{\delta_\infty} \leq 7.7 \times 10^6$.

The computed and experimental surface pressure is shown in Fig. 7. The calculated upstream propagation ΔX_p is 1.35 δ_∞, which is approximately 30% below the experimental value of 2.0 δ_∞. The underprediction of the upstream propagation at this Reynolds number $Re_{\delta_\infty} = 0.25 \times 10^6$ is consistent with the similar observation at $M_\infty = 3$ and $Re_{\delta_\infty} = 0.76 \times 10^6$. This implies that the necessary relaxation length is larger than δ_∞ for the present case, indicating that the relaxation length increases with decreasing Re_{δ_∞}. The computed profile is in general agreement with the experimental data downstream of the corner ($X > 0$).

6. Conclusions

The overall conclusions of the 2-D compression ramp studies are as follows (further discussion is presented in Ref. (16)):

a. The determination of the length and velocity scales of the eddy viscosity in outer region by the original Baldwin-Lomax model is unsuitable in the vicinity of separation. The model predicts an abrupt unphysical decrease in the turbulence length scale (by typically a factor of ten), resulting in a corresponding unphysical reduction in the magnitude of the eddy viscosity. A modified formulation for the length scale, proposed in the present study, provides some improvement, but does not eliminate the unphysical behavior.

b. The original and modified Baldwin-Lomax turbulence models exhibit an insufficient upstream propagation of the corner interaction.

c. A reasonably accurate prediction of the upstream propagation is achieved by incorporating a relaxation modification of the Baldwin-Lomax model. For the range of Reynolds numbers (Re_{δ_∞} = 0.76 x 10^6 to 7.7 x 10^6) and ramp angles (α = 8 deg to 24 deg) considered at Mach 3, a relaxation length equal to the upstream boundary layer thickness δ_∞ was found to predict ΔX_p within 20%. The agreement is excellent at the higher Reynolds numbers, with the discrepancy increasing with decreasing Re_{δ_∞}. This value of the relaxation length agrees with the previous results of Horstman et al. [10], using the Cebeci-Smith model, for the same Re_{δ_∞} and α range. The computed ΔX_p at Mach 2 for α = 16 deg, Re_{δ_∞} = 0.25 x 10^6 was approximately 30% below the experimental value. Since the extent of the upstream propagation increases with increasing relaxation length, the

results at Mach 2 and 3 suggest that the relaxation length is a moderate function of Re_{δ_∞} (i.e., the relaxation length increases with decreasing Re_{δ_∞} [17]). This observation is consistent with the results of Shang and Hankey [11] using the Cebeci-Smith model, who employed a relaxation length of 10 δ_∞ at Mach 3 for $Re_{\delta_\infty} = 0.14 \times 10^6$ and α = 15 to 25 deg.

d. All of the versions of the Baldwin-Lomax model fail to predict the observed rapid recovery of the boundary layer downstream of reattachment. This deficiency is attributable to the inability of the models to simulate the observed rapid amplification of the turbulent fluctuations [25,26] across a shock-turbulent boundary layer interaction.

e. The overall capability of the Baldwin-Lomax model for predicting 2-D turbulent interactions is comparable to other algebraic eddy viscosity models such as Cebeci-Smith.

B. Calculation of Three-Dimensional Supersonic Sharp Fin Flows

1. Objectives

The research effort on 3-D turbulent interactions has been guided over the past two years by the following objectives:

a. To examine the accuracy of theoretical predictions of 3-D shock wave-turbulent boundary layer interactions using the Baldwin-Lomax model.

This objective is a necessary prerequisite for utilizing the theoretical results to obtain greater understanding of the structure of 3-D turbulent interactions.

b. To evaluate the physical structure of the 3-D interaction flowfields using the computed results.

The principal effort during the first two years has been directed towards the "benchmark" computations needed to achieve the first objective. Within the second and third years, greater emphasis is placed on the evaluation of the physical structure of 3-D turbulent interactions.

2. Experimental Configuration

In choosing the flowfield configuration for the achievement of the stated objectives, several factors were considered including 1) the requirement for extensive experimental data (surface measurements and boundary layer profiles) for a range of Reynolds number Re_{δ_∞} and shock strength (i.e., pressure rise), 2) simplicity of geometry, and 3) interaction with the Princeton Gas Dynamics Laboratory. The experimental configuration chosen for theoretical investigation during the past two years is the 3-D sharp fin illustrated in Fig. 8. An oblique shock wave, generated by the deflection α_g of a sharp fin mounted perpendicular to a flat plate, intersects a supersonic equilibrium turbulent boundary layer which has developed on the flat plate. This

configuration has been investigated experimentally at various freestream conditions [27-35]. The theoretical effort has focused on several configurations at Mach 3 due to the extensive experimental data obtained by Oskam et al. [30-32] and McClure and Dolling [34,35] at the Princeton Gas Dynamics Lab. During the first two years, attention has been focused on flowfields at two different Reynolds numbers $Re_{\delta_\infty} = 2.8 \times 10^5$ and 9.32×10^5, and two different wedge angles $\alpha_g = 4$ and 10 deg. The available experimental data for these specific values of α_g is indicated in Table 3, and includes surface pressure and heat transfer, pitot pressure, yaw angle, pitch angle, total temperature and static pressure profiles.

3. Method of Solution

The governing equations are the full mean compressible Navier-Stokes equations in three dimensions using mass-averaged variables [15] and strong conservation form [9]. The molecular dynamic viscosity is determined by Sutherland's law. The molecular Prandtl number is 0.73 (air) and the turbulent Prandtl number is 0.9.

The two-layer algebraic turbulent eddy viscosity model of Baldwin and Lomax [5] is employed. The length scale in the inner layer is Buleev's mixing length [36,37]. The outer length and velocity scales are determined using the modified method utilized in previous studies [16,38]. The turbulence model constants specified by Baldwin and Lomax [5] are employed, with the exception that $C_{cp} = 2.08$. Previous numerical results [16,38] indicate that this value of C_{cp}, which is approximately 30% above the value given by Baldwin and Lomax, yields a more accurate prediction for a flat plate turbulent boundary layer at Mach 3. The turbulent eddy viscosity is implemented according to the method utilized by Hung and MacCormack [6] and Knight [38].

Conventional boundary conditions are specified on the surfaces of the

computational domain (Fig. 8). First, on the upstream boundary ABHG, the flow variables are held fixed at conditions corresponding to a developed flat plate boundary layer whose momentum thickness is identical to the experimental value. Second, on the solid boundaries corresponding to the wedge and flat plate surfaces, the velocity vector is set equal to zero, the wall temperature is specified, and the normal gradient of the static pressure is set to zero [39-41]. Third, on the plane of symmetry AFLG, the normal component of the velocity is set to zero, and the normal derivative of the remaining flow variables is set to zero. Fourth, on the outer boundaries BCDJIH and HIJKLG, zero gradient conditions are employed. These boundaries are located sufficiently far from the 3-D interaction to insure that an asymptotic two-dimensional flow exists. In particular, this implies that the shock wave generated by the sharp fin passes through the downstream boundary. Fifth, on the downstream boundary EDJK, the conventional zero gradient extrapolation is applied.

The governing equations are solved by a hybrid explicit-implicit algorithm [38]. The method combines the explicit finite-difference algorithm of MacCormack [42,43] with the implicit Box Scheme of Keller [44]. The Box Scheme is applied to the asymptotic form of the Navier-Stokes equations in the extremely thin portion of the turbulent boundary layer defined by the viscous sublayer and transition wall region. This narrow region is denoted the "computational sublayer" and is typically less than five percent of the local boundary layer thickness. The explicit algorithm of MacCormack is applied to the remainder of the physical computational domain. The utilization of an implicit method in the viscous sublayer and transition wall region of the boundary layers overcomes the severe time step constraint encountered by application of explicit methods to this region of the flow. Based upon previous study [38,39,45-47], the computational sublayer height z'_m is taken to be less

than 60 local wall units (i.e., $z_m'^+ \leq 60$, where $z_{m'+} = z_m' u_*/\nu_w$, u_* is the wall friction velocity, and ν_w is the wall kinematic viscosity).

The hybrid algorithm has been applied to a variety of two-dimensional [39,45,46] and three-dimensional [38,47] flows exhibiting shock-boundary layer interaction and flow separation. The implementation of the algorithm in three dimensions is discussed in detail in Ref. 38. The algorithm has been vectorized on the CYBER 203 computer at NASA Langley using the vector-processing language SL/1. The code employs the data management architecture of Smith and Pitts [48] based on an interleaved data base [49]. The algorithm provides a substantial improvement in efficiency compared to a vectorized version of MacCormack's algorithm alone. Benchmark studies [38] have shown the present algorithm to be a factor of 16 to 21 times faster than a vectorized, time-split operator version of MacCormack's explicit algorithm.

A boundary-fitted numerical grid, generated by a combination of geometrically-stretched and uniformly-spaced mesh points, was utilized for each calculation. The mesh points were distributed in a highly non-uniform manner, with refined spacing in the vicinity of the solid boundaries. The number of grid points varied depending upon the case, with a minimum of 28,230 for $\alpha_g = 4$ deg at $Re_{\delta_\infty} = 9.3 \times 10^5$, and a maximum of 106,316 for $\alpha_g = 10$ deg at $Re_{\delta_\infty} = 2.8 \times 10^5$. The normal mesh spacing adjacent to the solid boundaries was chosen to accurately resolve the viscous sublayer, and typically 17 points were contained within the boundary layer. Full details of the grid distribution for the $Re_{\delta_\infty} = 9.3 \times 10^5$ cases is provided in Ref. 38.

A total of five (5) cases have been computed over the combined first and second year of the research program. The specific cases are listed in Table 4. It is noted that comparison has been made with essentially <u>all</u> of the experimental data for these cases by McClure [34] and Oskam [32].

4. Brief Review of Results for First Year - (1 Oct. 1981 - 30 Sept. 1982)

During the first year of the research effort, the principal focus of the 3-D intersection study was the computation of the 3-D sharp fin flows at Reynolds number $Re_{\delta_\infty} = 9.3 \times 10^5$, and comparison with the extensive data of Oskam, which was obtained in spanwise planes oriented normal to the upstream flow (Fig. 9). As indicated in Table 4, computations were performed for two ramp angles, i.e., $\alpha_g = 4$ and 10 deg. The results of these computations have been discussed in the Annual Scientific Report for the first year [24]. The overall conclusions of the first and second years' study are included in Section II.B.6 below.

5. Summary of Results for Second Year - (1 Oct. 1982 - 30 Sept. 1983)

The principal emphases of the second year's effort for the 3-D sharp fin were the following:

a. Calculation of the $\alpha_g = 10$ deg configuration at Reynolds number $Re_{\delta_\infty} = 2.8 \times 10^5$ and comparison with the experimental data of McClure [34]. This configuration is denoted as Case 1.

b. Comparison of the computed results at $\alpha_g = 10$ deg and $Re_{\delta_\infty} = 9.3 \times 10^5$, obtained during the first year of the research effort, with the experimental data of McClure [34]. This configuration is denoted as Case 2.

The experimental flow conditions of McClure [34] are indicated in Table 5, and the flow conditions for the computations are indicated in Table 6. There is a 13.5% difference in the value of Re_{δ_∞} for Case 2 between the computation and the experiment. This is due to the fact that the freestream conditions in the computation for Case 2 were chosen to closely match the experimental conditions of Oskam [30-32].

The experimental data of McClure was obtained on streamwise planes at a

constant spanwise position as indicated in Fig. 10. This differs from the orientation of the data planes of Oskam shown in Fig. 9. The spanwise locations correspond to $z = 14.2\ \delta_\infty$ and $9.4\ \delta_\infty$, respectively, for Cases 1 and 2, where δ_∞ is given in Table 5.

The computation of the $\alpha_g = 10$ deg, $Re_{\delta_\infty} = 2.8 \times 10^5$ configuration was performed twice, using two separate numerical grids, denoted as "Grid No. 1" and "Grid No. 2". These mesh distributions differed only in the height of the computational sublayer adjacent to the flat plate. For Grid No. 1, the heigh was 29.2 wall units, based upon the upstream skin friction on the flat plate (i.e., $z_m'^+ = 29.2$, where $z_m'^+ = z_m' u_* / \nu_w$, where z_m' is the height of the computational sublayer, u_* is the local friction velocity, and ν_w is the wall kinematic viscosity). For Grid No. 2, $z_m'^+ = 46.2$ based upon the upstream flat plate skin friction. The computed solutions using Grid Nos. 1 and 2, therefore, allow determination of the sensitivity of the calculated solution to the height of the computational sublayer. Based upon previous 2-D investigations [39,45, 46], the computed results have been found insensitive to the height of the computational sublayer provided $z_m'^+ \leq 60$.

The computed and experimental pitot pressure profiles on the flat plate for Cases 1 and 2 are shown in Figs. 11 through 17. The vertical axis is the pitot pressure p_p, normalized by the upstream freestream pitot pressure p_{p_∞}. The horizontal axis is the distance normal to the flat plate, normalized by the upstream flat plate boundary layer thickness δ_∞ at $x = 0$ (see Table 5). The profiles are taken at a constant spanwise distance $z = 14.2\ \delta_\infty$ and $9.4\ \delta_\infty$, respectively, for Cases 1 and 2, where δ_∞ is given in Table 5. The streamwise location is given in terms of x_s/δ_0, where $x_s = (x - x_{shk})$, x_{shk} is the location of the theoretical inviscid shock wave at the specified spanwise location z, and δ_0 is the experimental flat plate boundary layer thickness measured at (x_{shk}, z) in the absence of the wedge. The shock location $x_{shk} = 12.0$ cm and

22.8 cm, respectively, for Cases 1 and 2. The local undistributed boundary layer thickness δ_0 is 0.59 cm and 1.55 cm, respectively. The figures are arranged with increasing x_s, with profiles from Cases 1 and 2 paired at approximately the same values of x.

In Figs. 11a and 11b, the pitot pressure profiles are shown at x_s/δ_0 = -8.98 and -5.84, respectively, for Cases 1 and 2. These locations are upstream of the 3-D turbulent interaction, and the computed and measured profiles are in close agreement. In Figs. 12a and 12b, pitot profiles are displayed at x_s/δ_0 = -1.71 and -1.76, respectively. Although this location is upstream of the theoretical inviscid shock, there exists a substantial overshoot in the pitot pressure [30-32,34] associated with the upstream propagation of the interaction. The comparison between the computed and experimental profiles is generally good, with the peak value of p_p predicted within 3.2% for Case 1 and 10.0% for Case 2. In Figs. 13a and 13b, the profiles are shown at x_s/δ_0 = -0.63 and -0.78, respectively. The peak value of p_p is again accurately predicted for Case 1, with a discrepancy of 5.9% between the computations and the experiment. The overshoot in p_p is also evident in the computed results for Case 2, although the difference in the computed and measured peak p_p is 17.7%.

The computed and experimental pitot profiles at x_s/δ_0 = 1.00 and 1.27, respectively, are shown in Figs. 14a and 14b. There is generally good agreement between the theory and experiment, although the computed profile near the wall for Case 2 underpredicts the observed p_p behavior. In Figs. 15a and 15b, results are displayed at x_s/δ_0 = 4.23 and 3.4, respectively (the profile at x_s/δ_0 = 3.4 is the farthest downstream experimental data for Case No. 2). The predicted and measured profiles are again seen to be in good agreement, except close to the wall in Case No. 2.

The continued development of the boundary layer pitot pressure profiles

for Case 1 ($Re_{\delta_\infty} \approx 2.8 \times 10^5$) is indicated in Figs. 16 and 17, corresponding to $x_s/\delta_0 = 14.2$ and 20.7, respectively. Although the theory underpredicts the measured p_p profile by typically 10% at $x_s/\delta_0 = 14.2$, the computed results at $x_s/\delta_0 = 20.7$ are in close agreement with the experiment.

The computed results for Case No. 1 using Grids No. 1 and 2 are seen to be in excellent agreement with each other. This result, together with a similar observation for the yaw angle (see below), verified the insensitivity of the computed flowfield to the height of the computational sublayer, within the restriction $z_m'^+ \leq 60$ as discussed previously.

The computed and measured yaw angle profiles are indicated in Figs. 18 to 24, where the yaw angle is $\tan^{-1}(w/u)$ (see Fig. 8). In Figs. 18a and 18b, the yaw angle profiles at $x_s/\delta_0 = -8.98$ and -5.84, respectively, for Cases 1 and 2 are shown. As indicated previously, these locations are upstream of the 3-D turbulent interaction, and the yaw angle is essentially zero. In Figs. 19a and 19b, the theoretical and experimental yaw profiles at $x_s/\delta_0 = -1.71$ and -1.76, respectively, are shown. Generally good agreement is obtained over most of the boundary layer, except near the wall ($y/\delta_\infty \leq 0.2$) where the computed profile underpredicts the measured yaw angles. In Figs. 20a and 20b, the profiles are displayed at $x/\delta_0 = -0.63$ and -0.78, respectively. In both cases, the experiment indicates an overshoot in the yaw angle for $y > \delta_\infty$ which is observed qualitatively in the computed profiles for Case 1 only at this station.

In Figs. 21a and 21b, the yaw angle profiles are shown at $x_s/\delta_0 = 1.00$ and 1.27, respectively. General good agreement is observed between the computation and experiment, although the computed profile for Case 2 underpredicts the measured profile near the wall. The asymptotic value of the yaw angle as y approaches zero is predicted reasonably well in both cases. In addition, the computed profiles accurately predict the "undershoot" in the

yaw angle profile outside the boundary layer (i.e., values of the yaw angle less than the wedge angle α_g = 10 deg). In Figs. 22a and 22b, the profiles are displayed at x_s/δ_0 = 4.23 and 3.4, respectively. The computed results are seen to be in reasonable agreement with the experiment, with the profile for Case 2 somewhat underpredicted near the wall.

The continued development of the yaw angle profile for Case 1 (Re_{δ_∞} = 2.8 x 10^5) is displayed in Figs. 23 and 24, corresponding to x_s/δ_0 = 14.2 and 20.7. The computed profiles are seen to be in close agreement with the experiment. The asymptotic experimental value of the yaw angle at the flat plate surface, which reached values as large as 40 deg at x_s/δ_0 = 1.27, decreases to 22 deg at x_s/δ_0 = 14.7, and 12 deg at x_s/δ_0 = 20.7. The computed asymptotic value of the yaw angle at x_s/δ_0 = 20.7 is 16 deg, which is within 4 deg of the measured value (the experimental uncertainty [34,35] is $\pm$ 1 deg).

Contour plots of the computed pitot pressure for Case 1 at various streamwise stations are displayed in Fig. 25. The plots display contours of p_p/p_{p_∞} at the following levels: 0.5, 0.7, 0.9, 1.1, 1.2, 1.3, 1.4, and 1.5. The streamwise stations are located at 2.54 cm (5.6 δ_∞) increments beginning at x = 0.51 cm. The plots are accurately scaled in the y-z plane, indicating that the width of the computational domain in the z-direction increased with distance x. The separation of the plots in the x-direction in Fig. 25, however, was chosen to provide maximum clarity, and does not represent the actual streamwise spacing.

The pitot pressure contours indicate the growth of the boundary layers on the flat plate and wedge surface. The shock wave is evident in the clustering of vertical pitot contours. The shock-capturing nature of the numerical algorithm effectively "diffuses" the shock wave over typically two to three grid points. The "bulge" in the pitot contours, extending to the right (i.e., increasing z-direction) at the intersection of the shock wave and

boundary layer on the flat plate, represents the upstream propagation of the 3-D turbulent interaction, and is observed in Figs. 12 and 13 as the "overshoot" in the pitot pressure. The particular contour p_p/p_{p_∞} = 1.4 displays a repeated U-shaped pattern in the region between the shock and the wedge surface and above the flat plate boundary layer. This pattern is associated with the small variations in p_p/p_{p_∞} around 1.4 in this inviscid region (p_p/p_{p_∞} varies between approximately 1.35 and 1.5 in this region), and does not represent a significant structure of the flow.

Contour plots of the computed pitch angle for Case 1 are displayed in Fig. 26 at the same streamwise stations. The pitch angle is defined as $\tan^{-1}(v/\mathrm{sqrt}(u^2+w^2))$, where (u,v,w) are the cartesian velocity components in the x,y and z directions, respectively. The contours are displayed at increments of 1 deg. The contour plots display a region of modest positive pitch angle in the vicinity of the intersection of the shock wave and the turbulent boundary layer on the flat plate, with a maximum value of approximately 4 deg. This maximum value decreases with x, and at the furthest downstream station is approximately 3 deg. In the vicinity of the corner formed by the flat plate and the wedge, a region of negative pitch angle is observed. Close to the leading edge, the minimum value of the pitch angle is approximately -10 deg (although not clearly visible in the contour plots). This region of negative pitch gradually disappears, and at the farthest downstream station the minimum value of the pitch angle is approximately -1 deg.

6. Conclusions

The overall conclusions of the 3-D sharp fin investigations to date are as follows:

a. The theoretical predictions using the Baldwin-Lomax algebraic

eddy viscosity model are in general agreement with the experimental data of Oskam and McClure for the 3-D sharp fin configuration at Mach 3 for the specific cases examined, i.e., α_g = 10 deg at $Re_{\delta_\infty} = 2.8 \times 10^5$, and α_g = 4 deg and 10 deg at $Re_{\delta_\infty} = 9.3 \times 10^5$.

The computed results have been compared with extensive experimental data for surface pressure and heat transfer, and profiles of pitot pressure, yaw angle, ptich angle, and static pressure profiles. In particular, the calculated results for α_g = 10 deg, $Re_{\delta_\infty} = 2.8 \times 10^5$ predict the recovery of the boundary layer downstream of the 3-D interaction with reasonable accuracy. This result is particularly important, in consideration of the inability of the Baldwin-Lomax model to accurately predict the recovery of the turbulent boundary downstream of the 2-D compression corner for separated flow conditions (see Section II.A.6).

b. The computed results have provided insight into the flow structure of the 3-D sharp fin turbulent interaction.

The favorable comparison between theory and experiment for the 3-D sharp fin has provided confidence in the accuracy of the numerical simulations. The computed results, therefore, can be employed to provide further understanding of the flow structure.

The contour plots of pitot pressure provide a clear picture of the physical structure associated with the "overshoot" in the pitot pressure outside the boundary layer and upstream of the shock. The pitch contours provide a qualitative and quantitative picture of the effect of the 3-D shock interaction

on the fluid motion. Efforts in numerical flow visualization are continuing in the present year of the research effort as discussed below.

7. Program Schedule for Third Year

The research program in 3-D turbulent interactions for the remainder of the third year is as follows:

a. Rewrite 3-D Navier-Stokes Code into CDC CYBER Fortran

The 3-D compressible Navier-Stokes code is currently written in the SL/1 computing language developed by John Knight at NASA Langley Research Center [50]. The SL/1 language is a powerful, vector-processing language which was designed especially for CYBER 203 application programming. In particular, the SL/1 language provides the capability of using a 32-bit word length. The CDC CYBER Fortran [51] developed by Control Data Corporation (the manufacturers of the CYBER 203) only provided a 64-bit word length until quite recently. The capability of 32-bit word length is extremely important, since a code written in 32-bit will execute approximately twice as fast as a code written in 64-bit, and will require one-half the central memory storage.

The 3-D Navier-Stokes code was written in SL/1 in order to take advantage of the increased execution speed and decreased storage requirements afforded by the language. Indeed, it would not have been possible to perform the computations discussed previously with the resources provided at NASA Langley if the code has been written in the 64-bit CDC CYBER Fortran.

However, recent developments at NASA Langley will require the rewriting of the 3-D Navier-Stokes code from SL/1 into the

recently-introduced 32-bit CDC CYBER 200 Fortran [52]. Specifically, NASA Langley will be installing Version 2.0 of the CYBER Operating System on the CYBER 203 within the next few months. This version of the operating system is not compatible with SL/1, and a decision has been made not to upgrade SL/1 to make it compatible with Version 2.0. It should be noted that, 1) SL/1 is available only at NASA Langley, 2) it is used by a relatively small number of individuals, and 3) the author of SL/1 (John Knight) is no longer at NASA Langley.

Several months are therefore planned for rewriting the 3-D Navier-Stokes code into CYBER 200 Fortran.

b. Calculation of 3-D Swept Compression Corner at Mach 3

A major focus of the third year is the computation of the 3-D swept turbulent compression corner configuration at Mach 3 for which extensive experimental data has been obtained by Settles and his colleagues at the Princeton Gas Dynamics Laboratory [53-55]. There are several goals of this research:

1) To evaluate the accuracy of the Baldwin-Lomax turbulence model for the 3-D swept turbulent compression corner configuration.

As discussed previously, the 3-D Navier-Stokes computations of the 3-D sharp fin flowfield using Baldwin-Lomax turbulence model were found to be in generally good agreement with the extensive experimental data obtained by the Princeton Gas Dynamics Laboratory. It is important, therefore, to examine the accuracy of the Baldwin-Lomax model for the 3-D swept turbulent compression corner configuration. Several of these

experimental configurations exhibit a significantly stronger interaction (e.g., larger static pressure rise) than the 10 degree 3-D sharp fin.

2) To examine the flow structure of the 3-D swept turbulent compression corner.

A significant effort will be focused on the development of numerical flow visualization techniques. These techniques will be applied to the understanding of the flow structure of this configuration. Due to the complexity of the 3-D flow structure, this aspect of the research is considered crucial.

3) To suggest further experiments to elucidate the flow structure of the 3-D swept turbulent compression corner.

The results of the computation may suggest further experiments for this configuration. For example, the surface pressure for the α_s = 24 deg, λ = 60 deg* configuration (which is in the conical flow regime) displays a marked peak on the corner line [55]. The computed results could be utilized to examine the nature of the flow structure(s) associated with this peak, and indicate specific regions of the flow for additional experimental investigation.

*The compression corner angle, measured in the streamwise direction, is denoted by α_s. The compression corner sweepback angle is denoted by λ.

C. Tables

TABLE 1: SUMMARY OF EXPERIMENTAL DATA FOR 2-D SUPERSONIC COMPRESSION RAMP AT MACH 3

Ramp Angle (degrees)	Re_{δ_∞}	Experimental Data
8	1.6×10^6	p_w, C_f, U, M, p
16	1.6×10^6	p_w, C_f, U, M, p
20	1.6×10^6	p_w, C_f, X_s, X_R, U, M, P
24	1.6×10^6	p_w, C_f, X_s, X_R, U, M, P
20	$.76 \times 10^6$	p_w, X_s, X_R
20	3.4×10^6	p_w, X_s, X_R
20	5.6×10^6	p_w, X_s, X_R
20	7.7×10^6	p_w, X_s, X_R

Legend:

p_w: wall static pressure
C_f: wall skin friction
X_s: separation point
X_R: reattachment point
U: velocity
M: Mach number profiles
p: static pressure profiles

TABLE 2: SUMMARY OF COMPUTATIONS FOR 2-D

COMPRESSION RAMP AT MACH 3

1 October 1981 - 30 September 1983

Re_{δ_∞}	Ramp Angle (α) degs.	No. of Computations		
		Model 1	Model 2	Model 3
1.6×10^6	8	4	0	0
	16	1	2	1
	20	1	1	1
	24	0	1	1
0.76×10^6	20	0	0	1
3.4×10^6	20	0	0	1
5.6×10^6	20	0	0	1
7.7×10^6	20	0	0	1
Total No. of Computations		6	4	7

Legend:

Model 1 : Original Baldwin-Lomax model

Model 2 : Modified Baldwin-Lomax model

Model 3 : Baldwin-Lomax model with Relaxation

TABLE 3: SUMMARY OF EXPERIMENTAL DATA OF OSKAM AND McCLURE FOR THE 3-D SHARP FIN AT SELECTED α_g

Re_{δ_∞}	Wedge Angle α_g (degs)	Ref.	Experimental Data
2.75×10^5	10	McClure [34]	p_s, p_p, yaw, vis
8.0×10^5	10	McClure [34]	p_s, p_p, yaw, vis
9.3×10^5	4	Oskam [32]	p_s, c_h, p_p, yaw p, T_t, pitch, vis
9.3×10^5	10	Oskam [32]	p_s, c_h, p_p, yaw, p, T_t, pitch, vis

Legend:

p_p : pitot pressure profiles

yaw : yaw angle profiles

p_s : surface pressure

c_h : surface heat transfer

p : static pressure profiles

T_t : total temperature profiles

pitch : pitch angle profiles

vis : surface flow visualization (oil or kerosene-graphite)

TABLE 4: SUMMARY OF COMPUTATIONS FOR 3-D SHARP FIN

1 October 1981 - 30 September 1983

Re_{δ_∞}	Wedge Angle α_g (degs)	No. of Computations
2.8×10^5	10	2
9.3×10^5	4	1
	10	2
	Total No. of Computations	5

TABLE 5: FLOW CONDITIONS FOR EXPERIMENTS OF McCLURE [34] FOR 3-D SHARP FIN

Case No.	δ_∞ (cm)	M_∞	α_g	Re_{δ_∞}	Total Pressure (kPa)	Total Temperature (deg K)
1	0.45	2.91	10.0	2.75×10^5	689.7	275.9
2	1.29	2.93	10.0	8.0×10^5	689.9	271.4

TABLE 6: FLOW CONDITIONS FOR COMPUTATIONS FOR

3-D SHARP FIN AT α_g = 10 deg

Case No.	δ_∞ (cm)	M_∞	α_g	Re_{δ_∞}	Total Pressure (kPa)	Total Temperature (deg K)
1	0.45	2.91	10.0	2.75×10^5	689.7	275.9
2	1.37	2.94	9.72	9.25×10^5	689.7	255.6

D. Figures

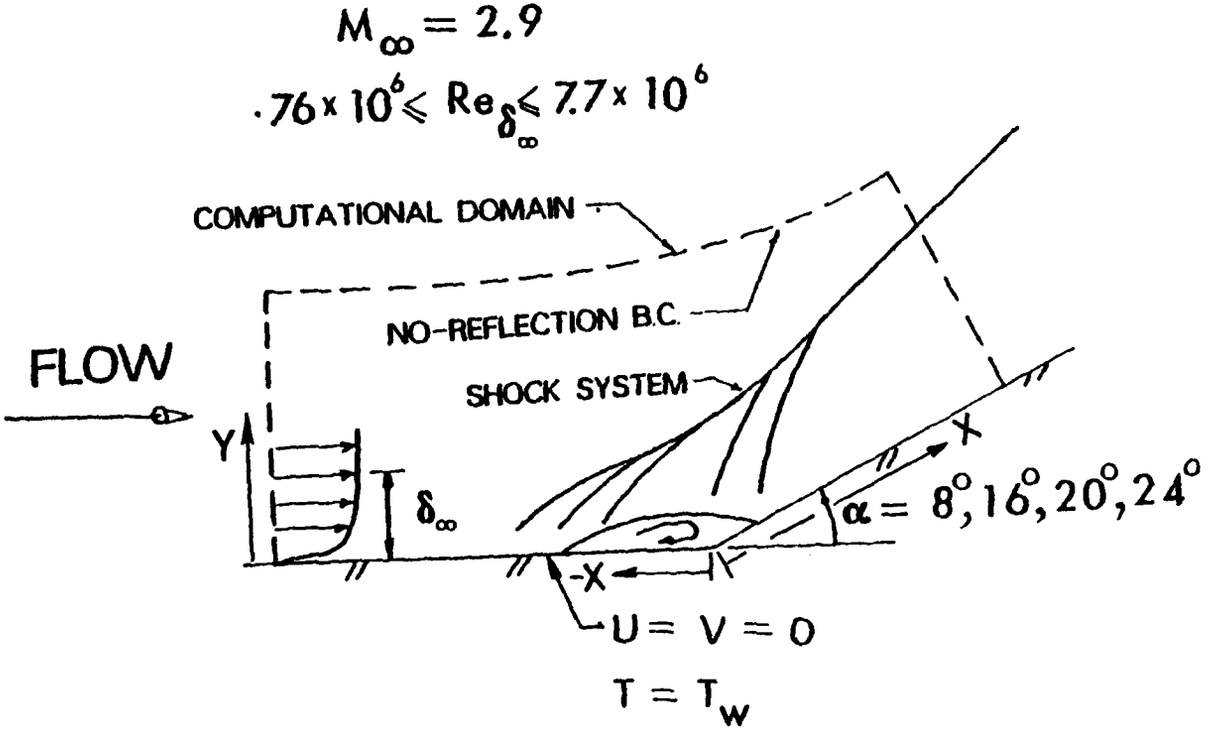

Fig. 1 - Geometry of 2-D Supersonic Compression Ramp

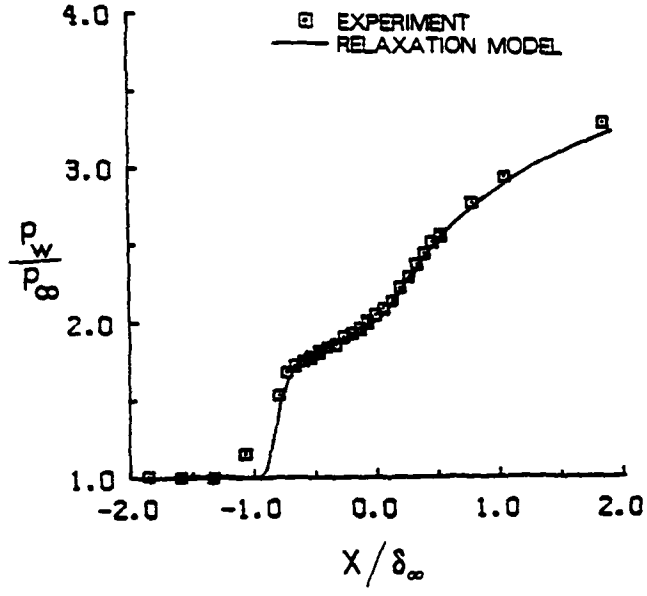

Fig. 2 Surface pressure for α = 20 deg, Re_{δ_∞} = 0.76 x 10^6 at M_∞ = 2.9.

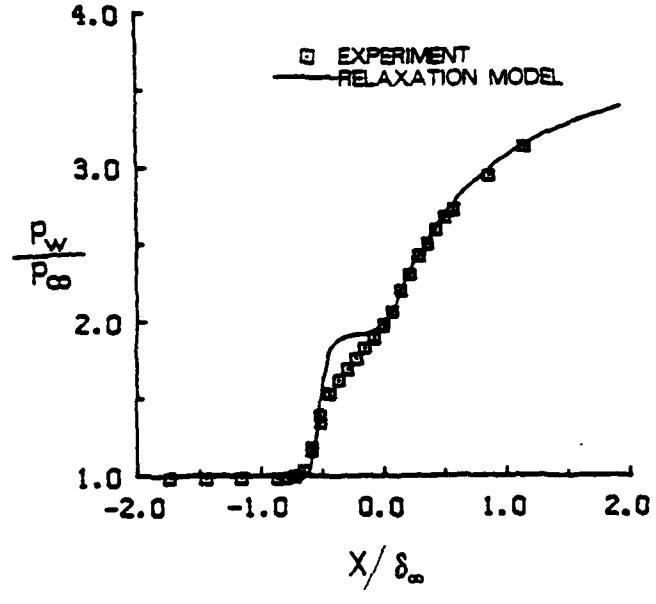

Fig. 3 Surface pressure for α = 20 deg, Re_{δ_∞} = 3.4 x 10^6 at M_∞ = 2.9

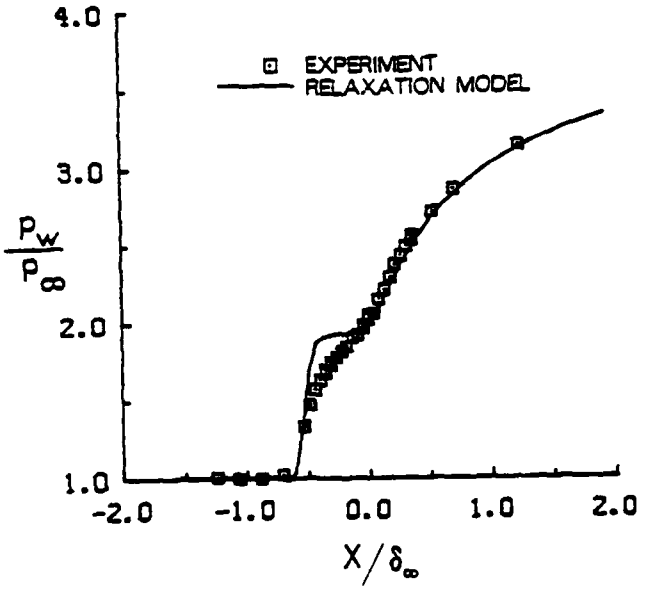

Fig. 4 Surface pressure for α = 20 deg, Re_{δ_∞} = 5.6 x 10^6 at M_∞ = 2.9

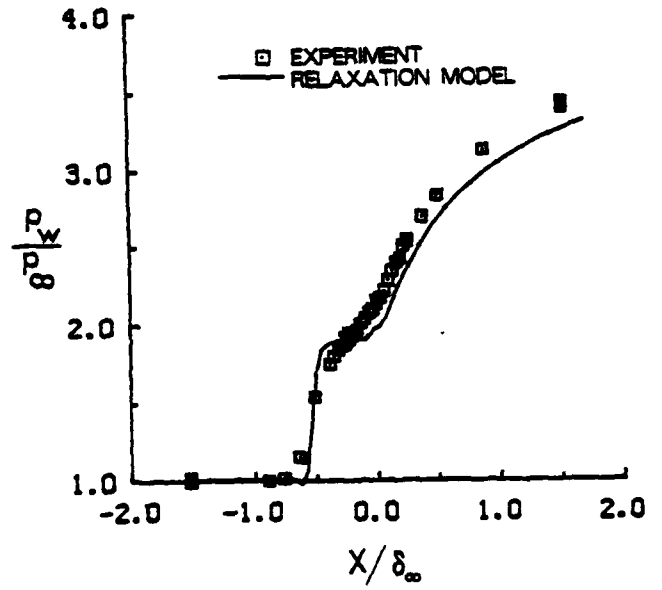

Fig. 5 Surface pressure for α = 20 deg, Re_{δ_∞} = 7.7 x 10^6 at M_∞ = 2.9

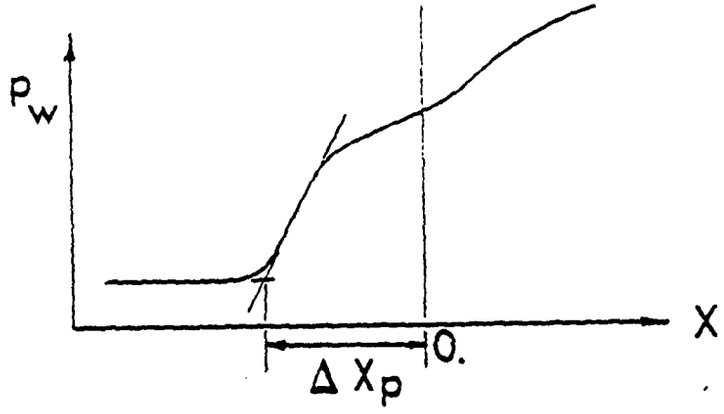

$$l_s = x_R - x_s$$

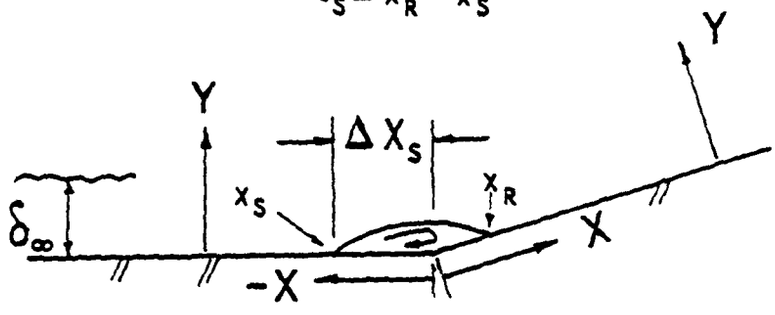

Fig. 6a Definition of Interaction Geometric Distances

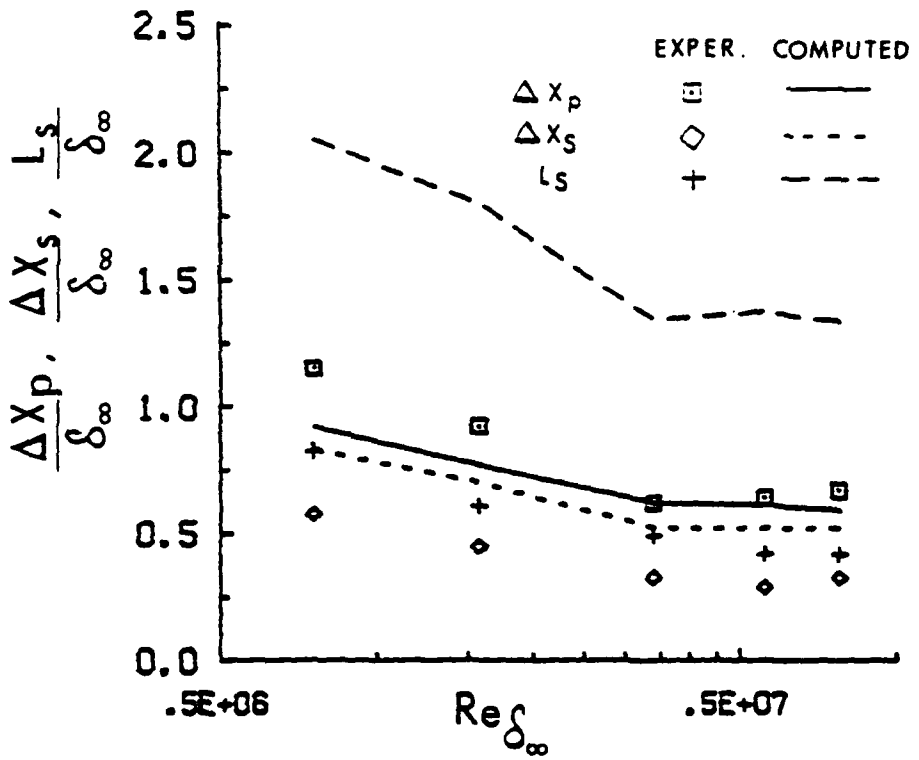

Fig. 6b Effect of Re_{δ_∞} on Interaction Lengths for α = 20 deg at M_∞ = 2.9

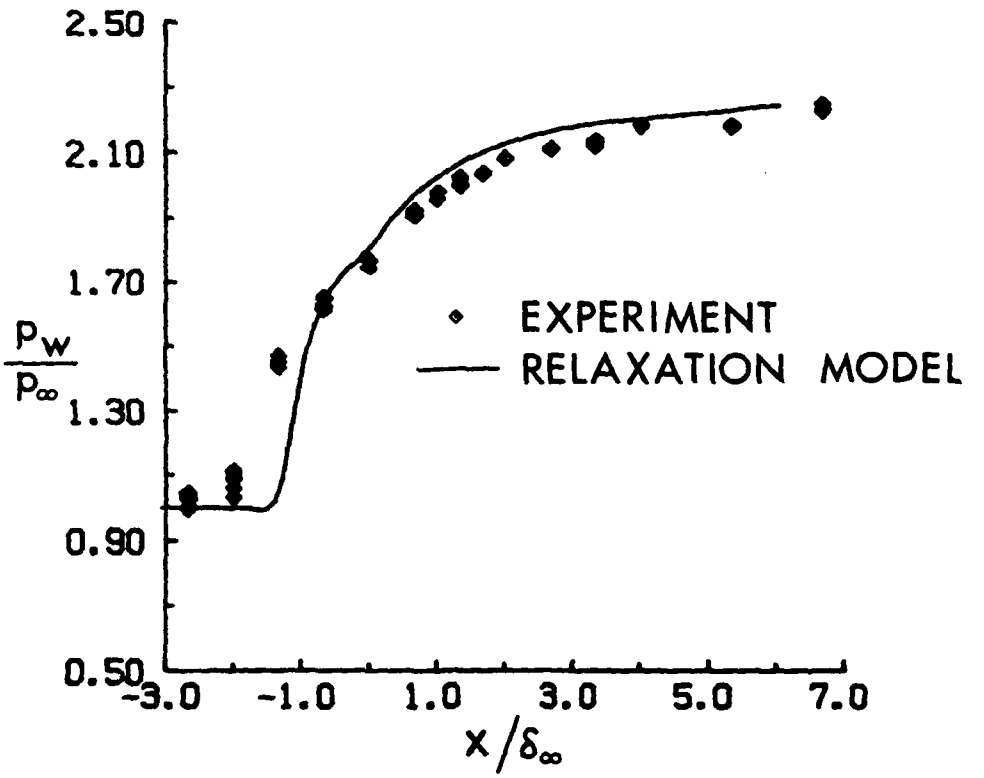

Fig. 7 Surface pressure for α = 16 deg, $Re_{\delta_\infty} = 0.25 \times 10^6$ at M_∞ = 1.96

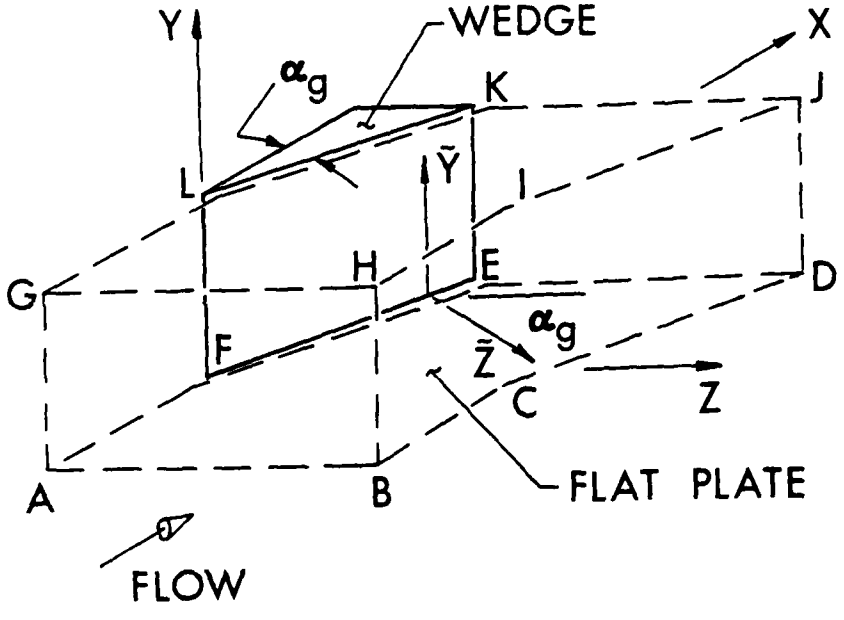

Fig. 8 Geometry of 3-D Supersonic Sharp Fin

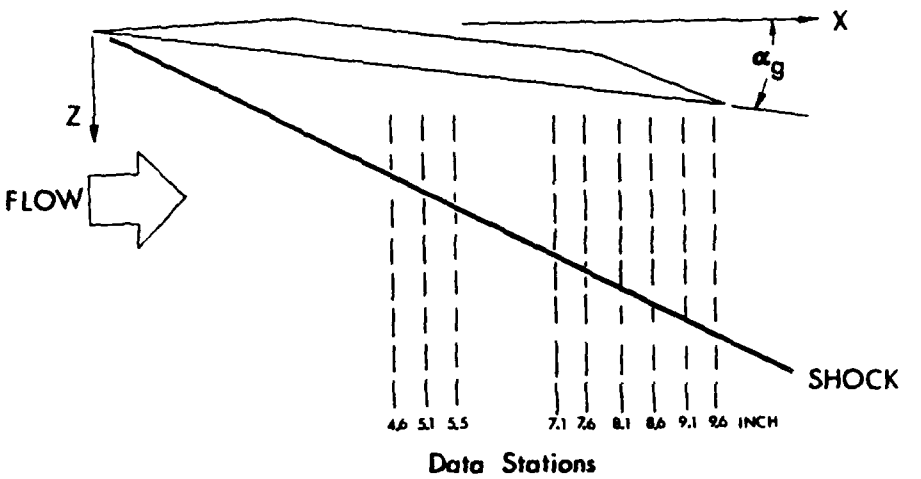

Fig. 9 Experimental Data Stations of Oskam

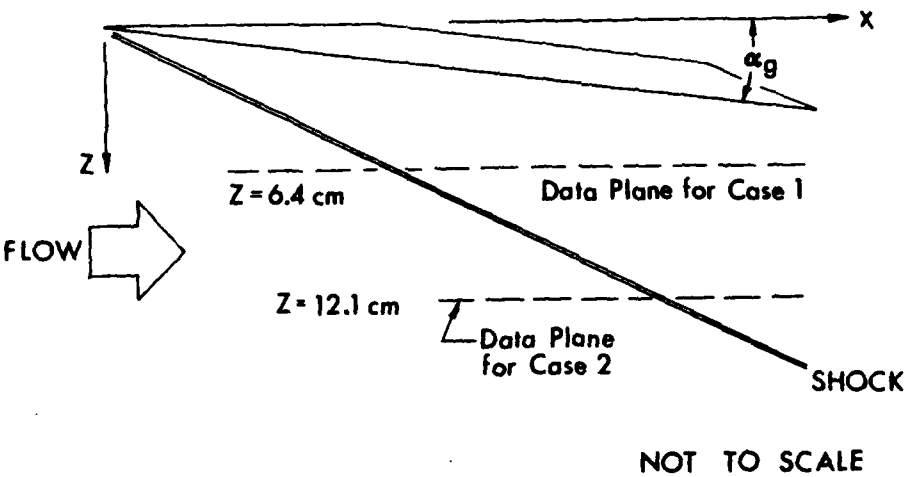

Fig. 10 Experimental Data Stations of McClure

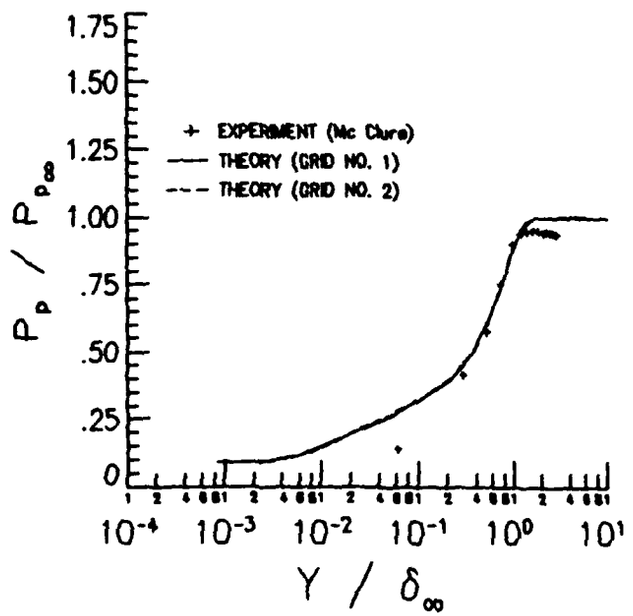

Fig. 11a Pitot pressure at x_s/δ_0 = -8.98 for Case 1

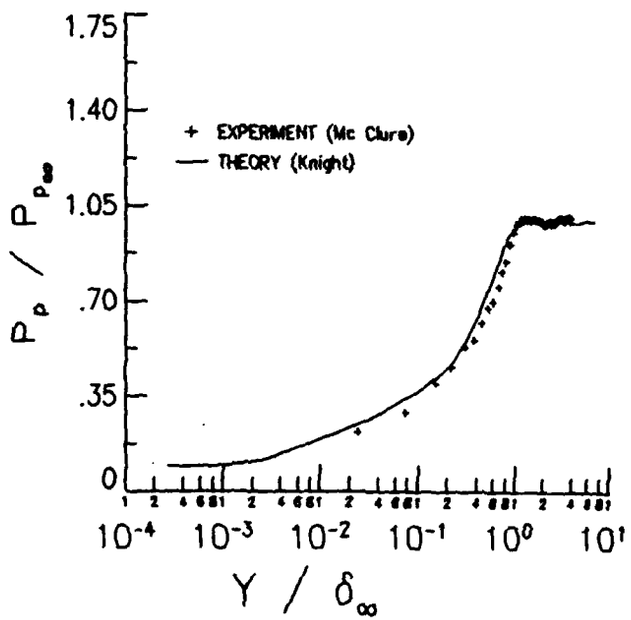

Fig. 11b Pitot pressure at x_s/δ_0 = -5.84 for Case 2

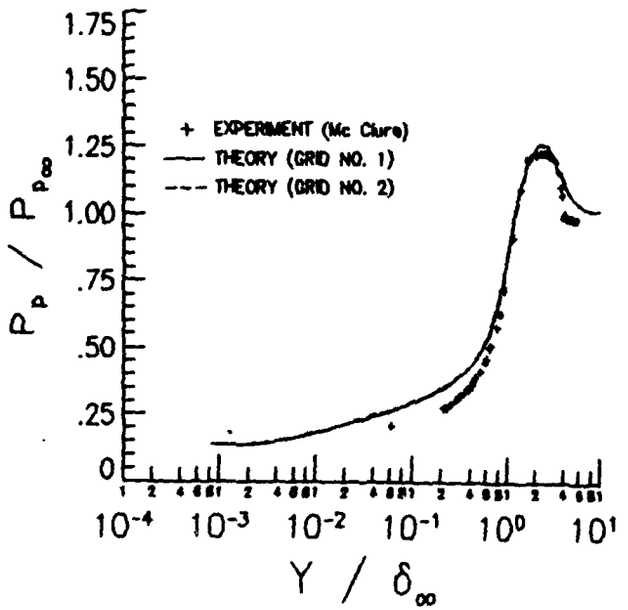

Fig. 12a Pitot pressure at x_s/δ_0 = -1.71 for Case 1

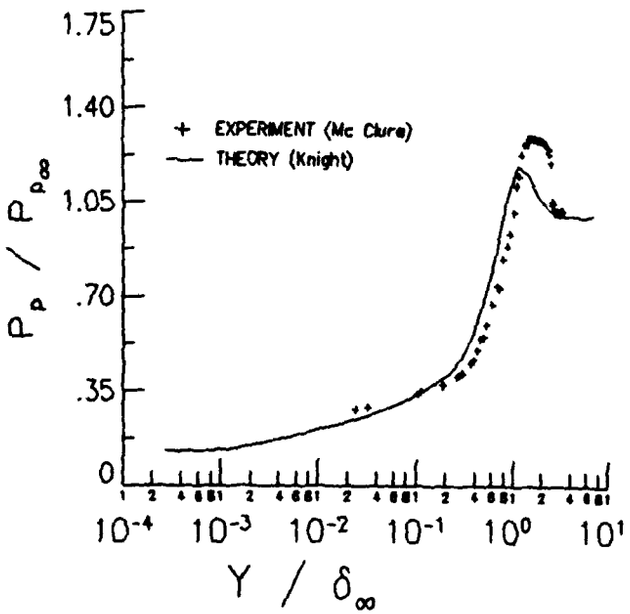

Fig. 12b Pitot pressure at x_s/δ_0 = -1.76 for Case 2

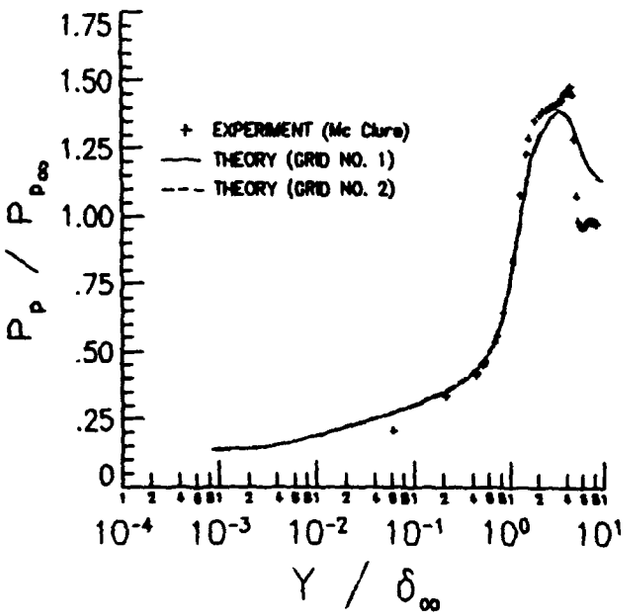

Fig. 13a Pitot pressure at $x_s/\delta_0 = -0.63$ for Case 1

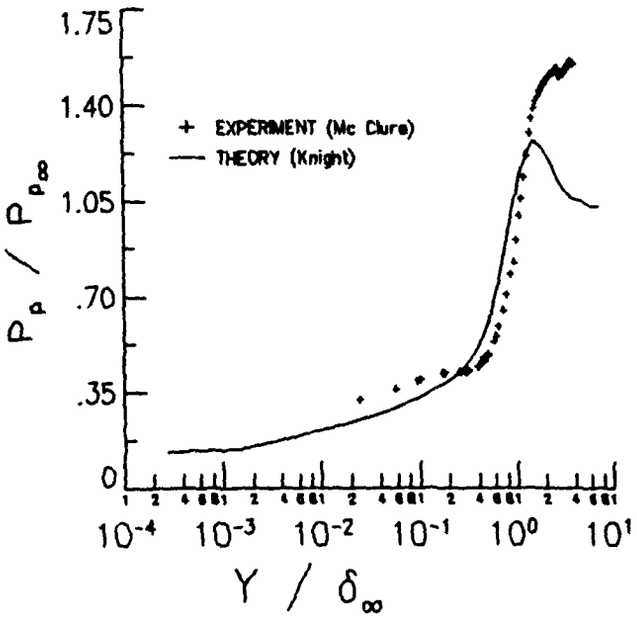

Fig. 13b Pitot pressure at $x_s/\delta_0 = -0.78$ for Case 2

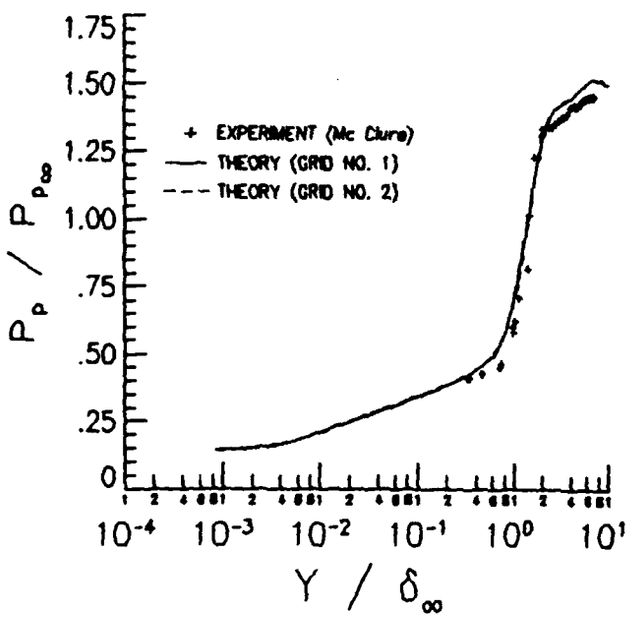

Fig. 14a Pitot pressure at $x_s/\delta_0 = 1.0$ for Case 1

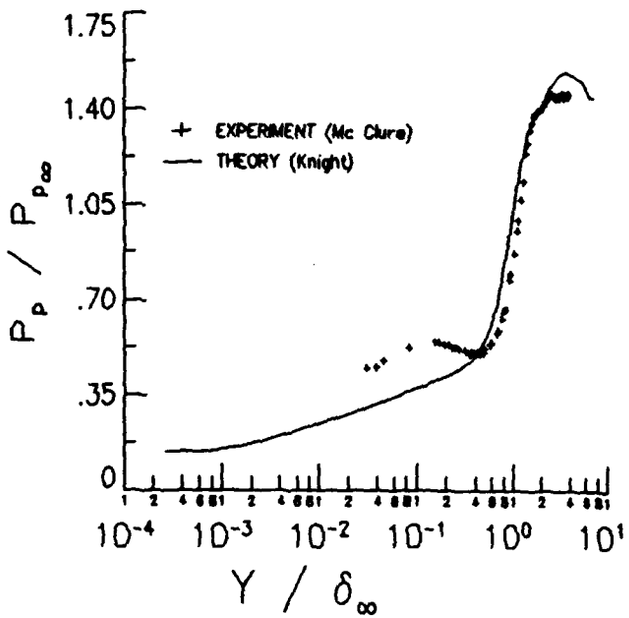

Fig. 14b Pitot pressure at $x_s/\delta_0 = 1.27$ for Case 2

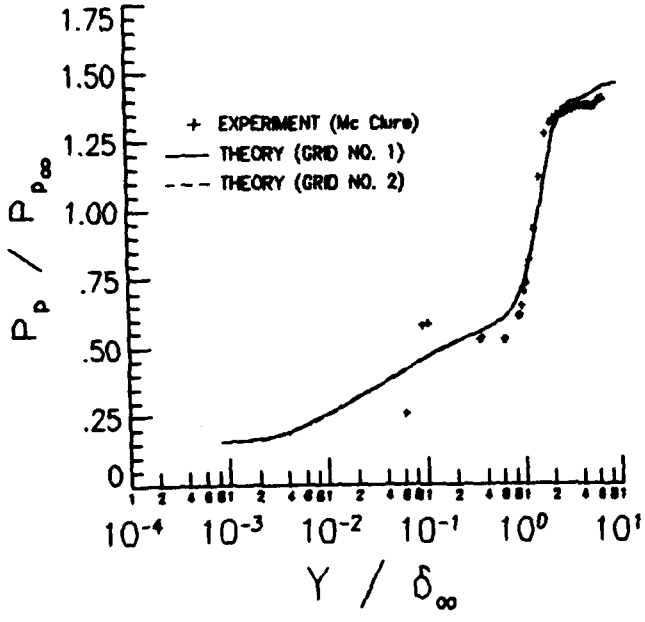

Fig. 15a Pitot pressure at $x_s/\delta_0 = 4.23$ for Case 1

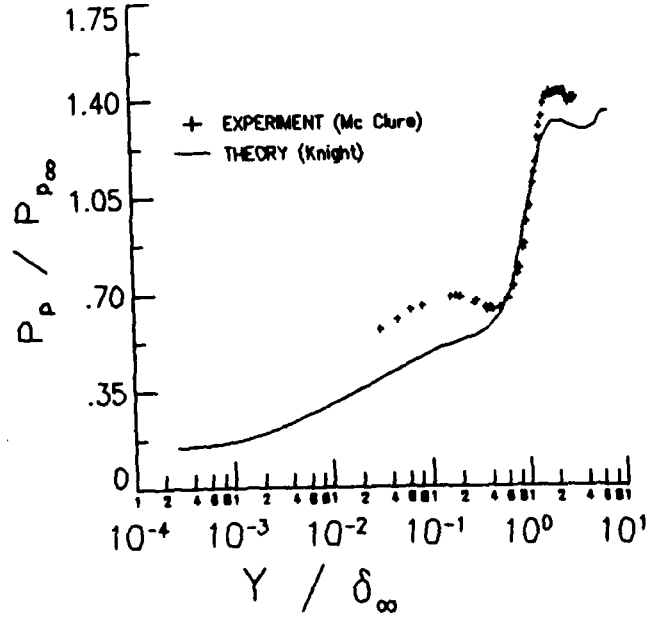

Fig. 15b Pitot pressure at $x_s/\delta_0 = 3.4$ for Case 2

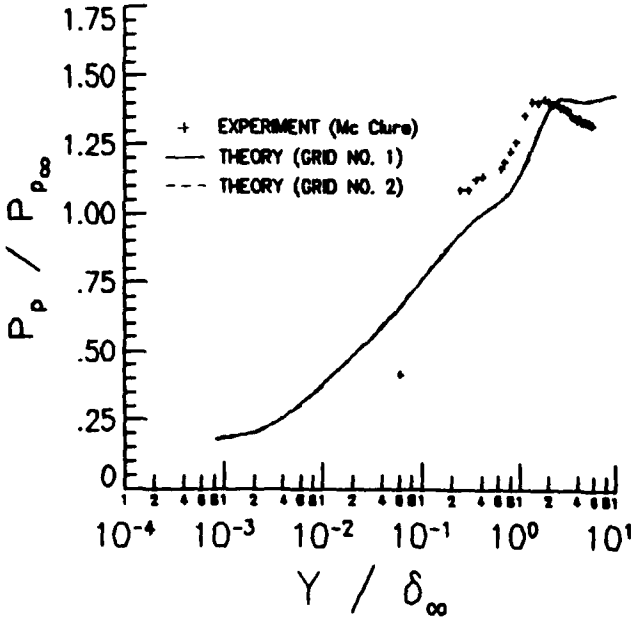

Fig. 16 Pitot pressure at x_s/δ_0 = 14.2 for Case 1

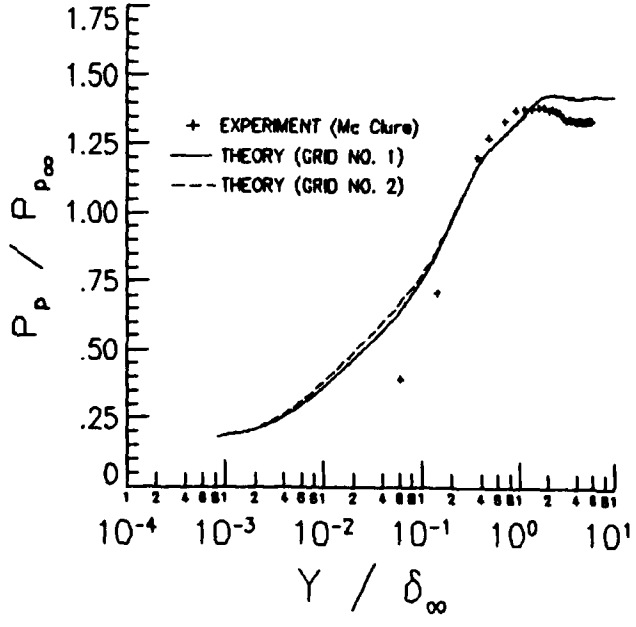

Fig. 17 Pitot pressure at x_s/δ_0 = 20.7 for Case 2

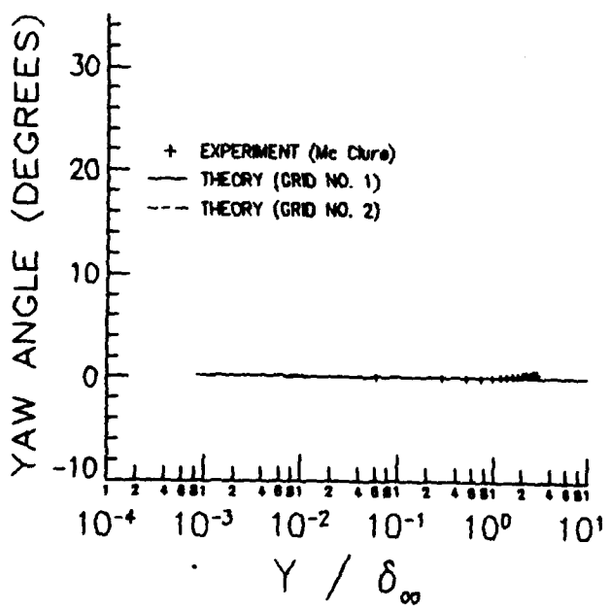

Fig. 18a Yaw angle at $x_s/\delta_0 = -8.98$ for Case 1

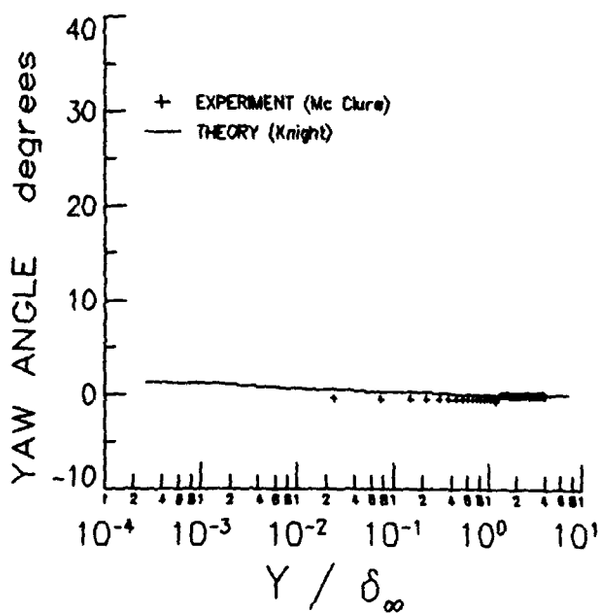

Fig. 18b Yaw angle at $x_s/\delta_0 = -5.84$ for Case 2

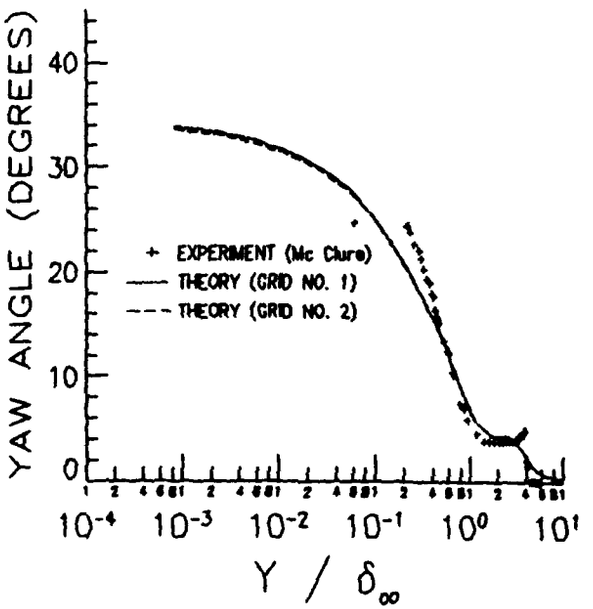

Fig. 19a Yaw angle at $x_s/\delta_0 = -1.71$ for Case 1

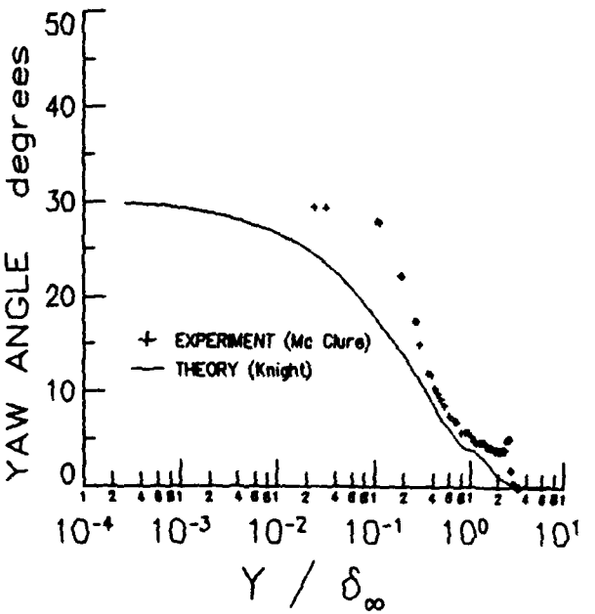

Fig. 19b Yaw angle at $x_s/\delta_0 = -1.76$ for Case 2

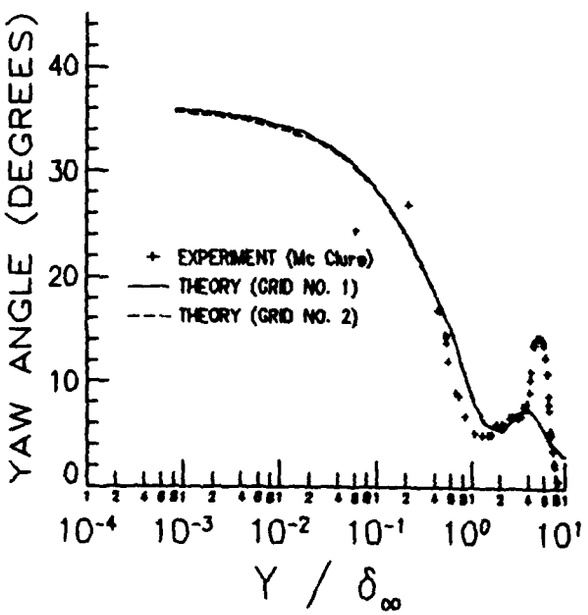

Fig. 20a Yaw angle at $x_s/\delta_0 = -0.63$ for Case 1

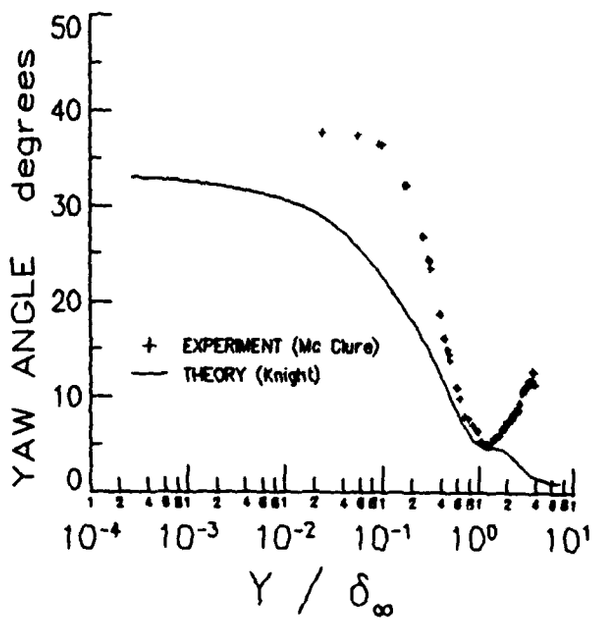

Fig. 20b Yaw angle at $x_s/\delta_0 = -0.78$ for Case 2

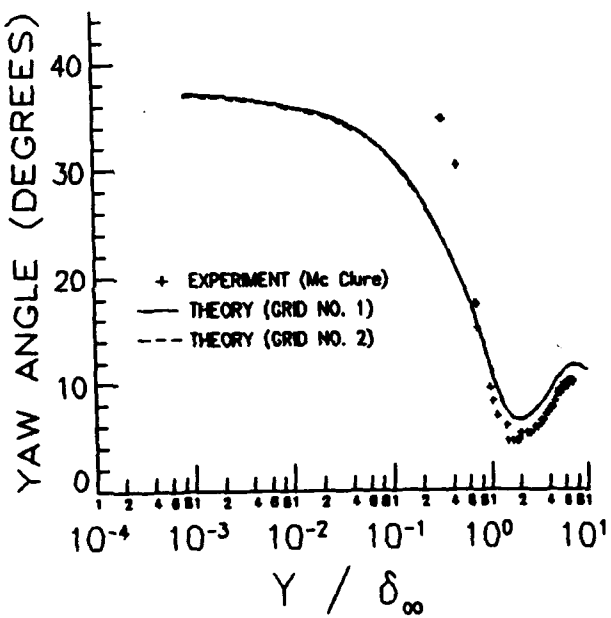

Fig. 21a Yaw angle at x_s/δ_0 = 1.0 for Case 1

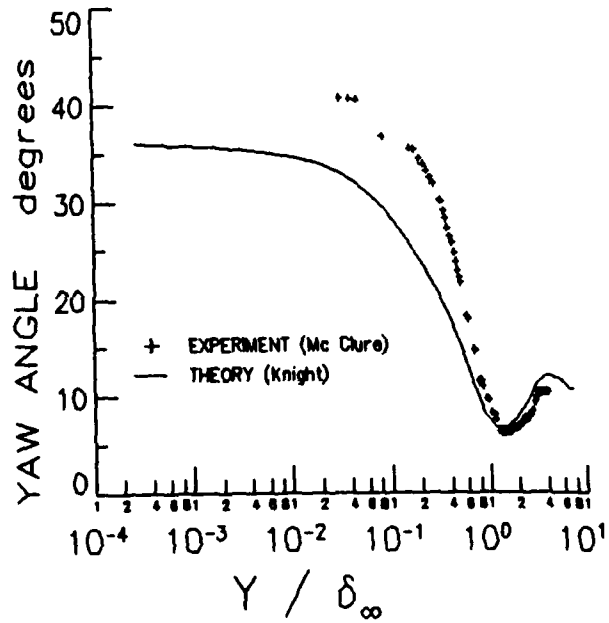

Fig. 21b Yaw angle at x_s/δ_0 = 1.27 for Case 2

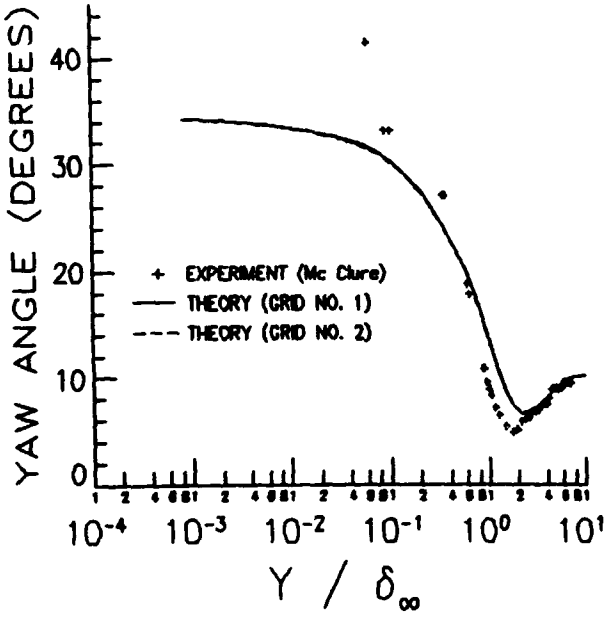

Fig. 22a Yaw angle at $x_s/\delta_0 = 4.23$ for Case 1

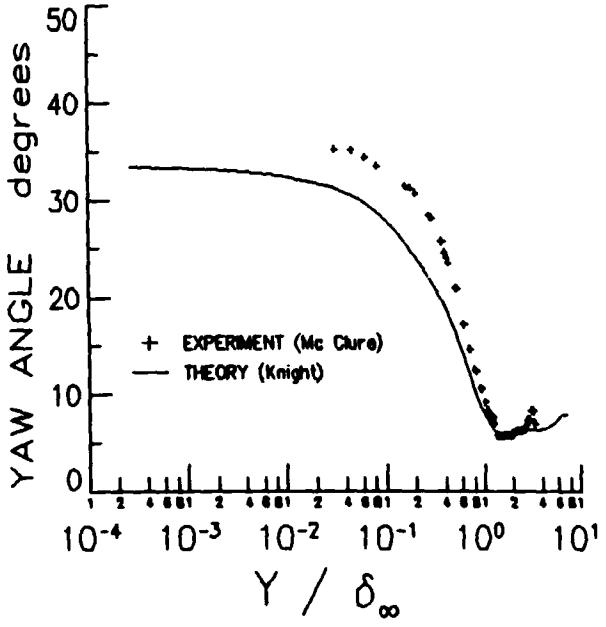

Fig. 22b Yaw angle at $x_s/\delta_0 = 3.4$ for Case 2

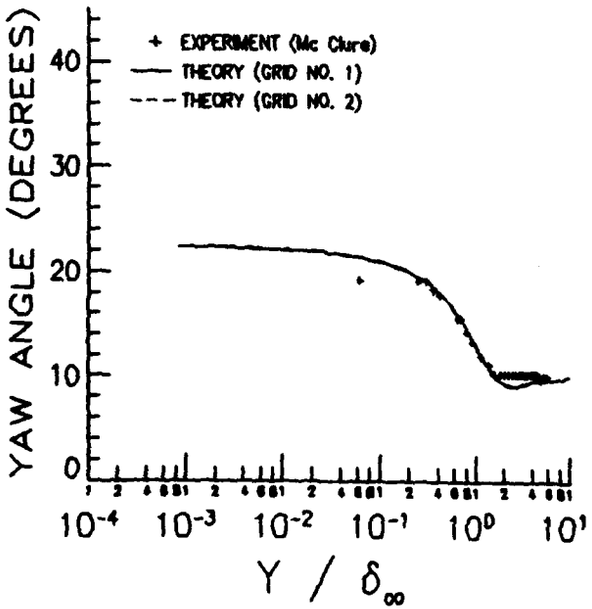

Fig. 23 Yaw angle at x_s/δ_0 = 14.2 for Case 1

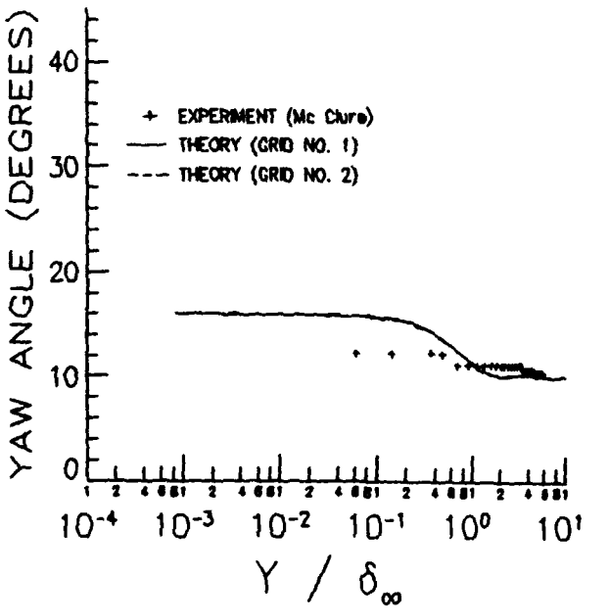

Fig. 24 Yaw angle at x_s/δ_0 = 20.7 for Case 2

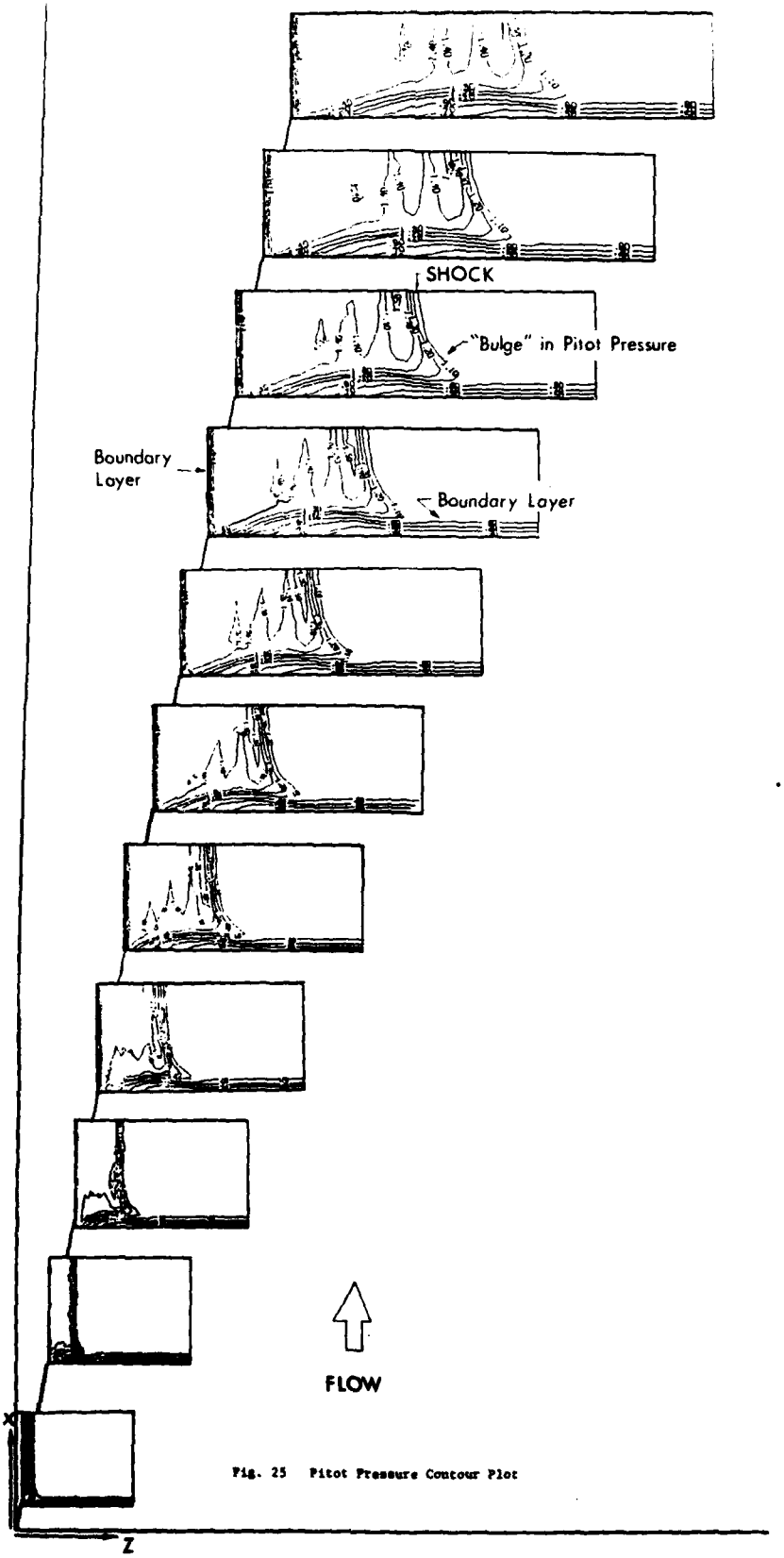

Fig. 25 Pitot Pressure Contour Plot

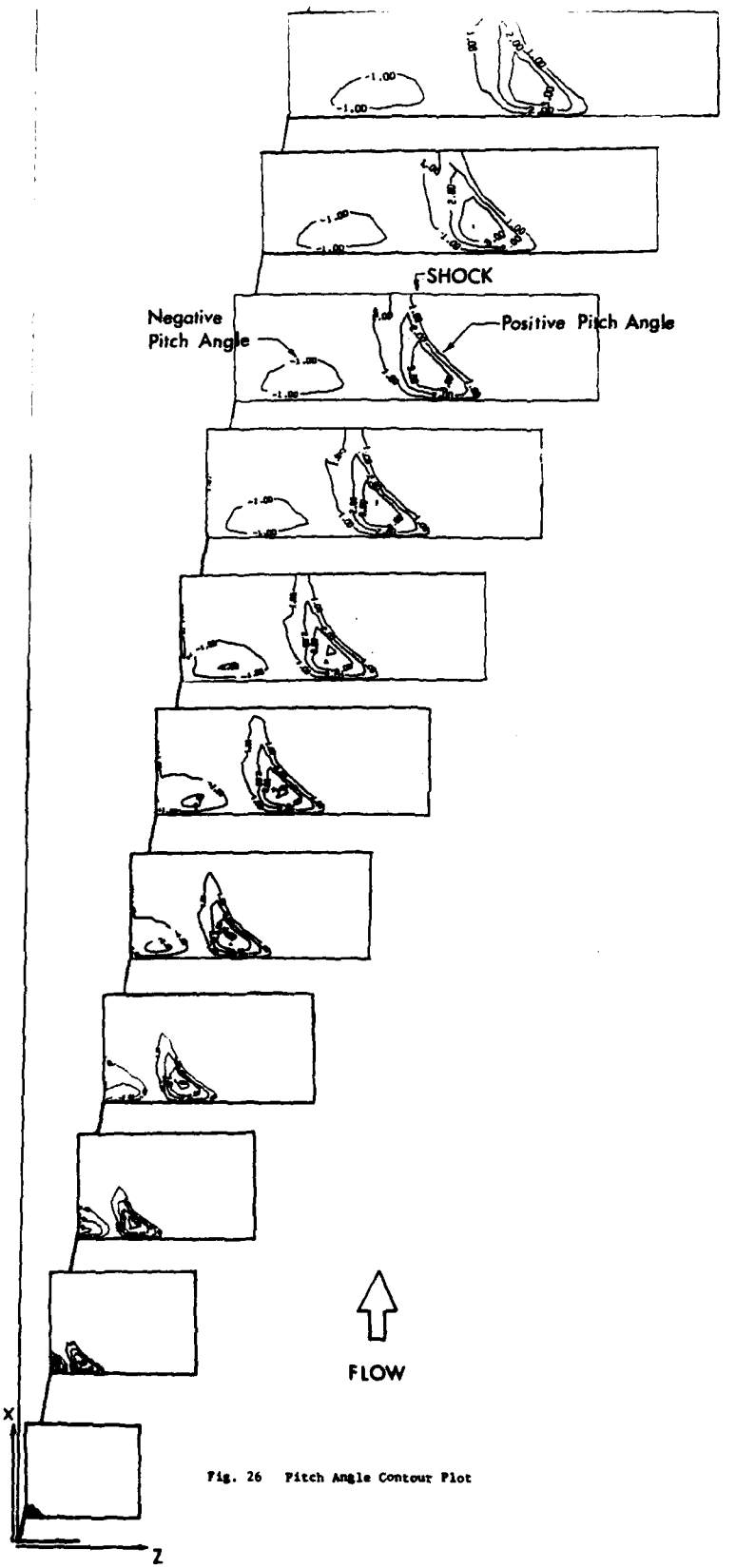

Fig. 26 Pitch Angle Contour Plot

III. Publications and Scientific Interactions

Period: 1 October 1982 to 30 September 1983

A. Written Publications

1. Knight, D., "A Hybrid Explicit-Implicit Numerical Algorithm for the Three-Dimensional Compressible Navier-Stokes Equations," AIAA Paper No. 83-0223, AIAA 21st Aerospace Sciences Meeting, Reno, Nevada, January 10-13, 1983 (research supported by AFOSR Grants ~~80-0072 and 82-0040~~ AFOSR-80-0072 & AFOSR-82-0040). Submitted for publication in the AIAA Journal.
2. Knight, D., "Calculation of a Simulated 3-D High Speed Inlet Using the Navier-Stokes Equations," AIAA Paper No. 83-1165, AIAA/SAE/ASME 19th Joint Propulsion Conference, Seattle, Washington, June 27-29, 1983 (research supported by AFOSR Grant ~~80-0072~~ AFOSR-80-0072). To be submitted for publication.
3. Visbal, M. and Knight, D., "Evaluation of the Baldwin-Lomax Turbulence Model for Two-Dimensional Shock Wave Boundary Layer Interactions," AIAA Paper No. 83-1697, AIAA 16th Fluid and Plasma Dynamics Conference, Danvers, Mass., July 12-14, 1983 (research supported by AFOSR Grant ~~82-0040~~ AFOSR-82-0040). Accepted for publication in the AIAA Journal.

B. Interactions with Research Group at Princeton Gas Dynamics Laboratory

1. Overview

Throughout the research program, close and continuous interaction has been maintained with the Research Group at the Princeton Gas Dynamics Laboratory. These individuals include Profs. S. Bogdonoff and L. Smits, and Drs. D. Dolling (presently at Univ. of Texas at Austin) and G. Settles (currently at Penn State

Univ.). The interaction has been manifested in two major areas, specifically:

a. Frequent Meetings with the Princeton Gas Dynamics Laboratory Research Group.

Frequent meetings have been held with the Princeton Gas Dynamics Laboratory Research Group. The purpose of these meetings has been to discuss the progress of the theoretical research, to seek greater understanding of the particular flow configuration, and to suggest future directions for the research effort. These meetings have been very productive, and a list of meetings held during the present research period is provided in the next section.

b. Computation of 2-D and 3-D Turbulent Interactions and Comparison with Experimental Data at Princeton Gas Dynamics Laboratory.

During the first twenty-four months of the research effort (1 October 1981 - 30 September 1983), efforts have been focused in two main areas, namely 1) the computation of 3-D supersonic sharp fin flows at Mach 3, and 2) the computation of 2-D supersonic turbulent compression corner flows at Mach 2 and 3. Since all of the experimental data for these configurations was obtained at the Princeton Gas Dynamics Laboratory, a close interaction was obtained in the discussion of the computed results.

2. Schedule of Meetings with Princeton Gas Dynamics Laboratory Research Group from 1 October 1982 to 1 November 1983

a. 19 October 1982: Meeting at Princeton Gas Dynamics Lab

Topics: 1) Discussion of computed results to date for 2-D supersonic compression corner at Mach 3.

2) Discussion of computed results for 3-D sharp

fin at Mach 3 and $Re_{\delta_\infty} = 9.3 \times 10^5$ and comparison with experimental data of McClure.

3) Discussion of computed results for 3-D sharp fin at Mach 3 and $Re_{\delta_\infty} = 9.3 \times 10^5$ and comparison with experimental data of Oskam.

4) Discussion of future work.

b. 27 October 1982: Meeting with Dr. G. Settles at Rutgers University

Topics: 1) Discussion of computed results to date for 2-D supersonic compression corner at Mach 3.

c. 13 December 1982: Meeting at Princeton Gas Dynamics Lab with Research Group and Dr. J. Wilson (AFOSR)

Topics: 1) Discussion of computed results to date for 2-D and 3-D turbulent interactions at Mach 3.

2) Discussion of experimental results for 2-D and 3-D turbulent interactions.

3) Presentation of future plans.

d. 1 February 1983: Meeting at Princeton Gas Dynamics Lab

Topics: 1) Discussion of experimental results for 2-D and 3-D turbulent interactions at Mach 2 obtained at Gas Dynamics Lab.

2) Discussion of future computation of 2-D supersonic compression corner at Mach 2 for comparison with Gas Dynamics Lab data.

3) Discussion of inadequacies of Baldwin-Lomax turbulence model for 2-D turbulent interactions.

e. 17 February 1983: Meeting with Prof. S. Bogdonoff at Princeton

Topics: 1) Discussion of flow structure of 3-D sharp fin interaction.

2) Discussion of possible approaches to numerical

flow visualization of 3-D sharp fin interaction.

f. 5 April 1983: Meeting at Princeton Gas Dynamics Lab

Topics: 1) Discussion of experimental results for 2-D supersonic compression corner at Mach 2.

2) Decision made on specific case of 2-D supersonic compression corner at Mach 2 for computation.

g. 13 April 1983: Meeting with Prof. S. Bogdonoff at Rutgers University

Topics: 1) Discussion of flow structure of 3-D sharp fin interaction.

2) Discussion of possible future theoretical and experimental investigations.

h. 12 May 1983: Meeting at Princeton Gas Dynamics Lab

Topics: 1) Discussion of theoretical and experimental research program for remainder of present year, and plans for next year.

i. 25 October 1983: Meeting at Princeton Gas Dynamics Lab

Topics: 1) Discussion of computed results of 3-D sharp fin at $Re_{\delta_\infty} = 2.8 \times 10^5$.

2) Discussion of recent experiments on 3-D sharp fin at Princeton.

3) Discussion of possible future 3-D turbulent interaction computations.

C. Spoken Papers Presented at Technical Meetings, 1 October 1982 - 30 September 1983

1. Knight, D., "Computation of Three-Dimensional Shock Wave Turbulent Boundary Layer Interaction," Thirty-Fifth Annual Meeting, Division of Fluid Dynamics, American Physical Society, Rutgers University,

New Brunswick, New Jersey, November 21-23, 1983; Bulletin of the American Physical Society, Vol. 27, No. 9, November 1982, p. 1190.

2. Visbal, M. and Knight, D., "Evaluation of the Baldwin-Lomax Turbulence Model for 2-D Shock-Turbulent Boundary Layer Interactions," Thirty-Fifth Annual Meeting, Division of Fluid Dynamics, American Physical Society, Rutgers University, New Brunswick, New Jersey, November 21-23, 1982; Bulletin of the American Physical Society, Vol. 27, No. 9, November 1982, p. 1162.

D. Seminars

1. Knight, D., "Numerical Simulation of 3-D Shock Wave-Turbulent Boundary Layer Interaction Using the CYBER 203 Vector-Processing Computer," Department of Aerospace and Mechanical Engineering, Princeton University, April 5, 1983.
2. Knight, D., "Numerical Simulation of 3-D Oblique Shock Wave Turbulent Boundary Layer Interaction," Department of Aerospace Engineering, University of Maryland, April 15, 1983.

IV. List of Personnel and Degrees Awarded

A. Personnel

Principal Investigator: Prof. Doyle Knight
Department of Mechanical and
Aerospace Engineering

Graduate Research Assistant: Mr. Miguel Visbal
Department of Mechanical and
Aerospace Engineering

Mr. Brian York
Department of Mechanical and
Aerospace Engineering

B. Degrees Awarded

Miguel R. Visbal

Ph.D., Mechanical and Aerospace Engineering, October 1983

Thesis title: "Numerical Simulation of Shock/Turbulent Boundary Layer Interactions over 2-D Compression Corners"

Thesis advisor: Prof. Doyle Knight

V. References

1. Green, J., "Interactions Between Shock Waves and Turbulent Boundary Layers," Prog. Aero. Sciences, Vol. 11, 1970, pp. 235-340.

2. Hankey, W. and Holden, M., "Two-Dimensional Shock Wave-Boundary Layer Interactions in High Speed Flows," AGARDograph No. 203, June 1975.

3. Christiansen, W., Russell, D., and Hertzberg, A., "Flow Lasers," Annual Review of Fluid Mechanics, Vol. 7, 1975, pp. 115-140.

4. Knight, D., "Theoretical Investigation of Three-Dimensional Shock Wave-Turbulent Boundary Layer Interactions," Research Proposal submitted to the Air Force Office of Scientific Research, June 1981.

5. Baldwin, B. and Lomax, H., "Thin Layer Approximation and Algebraic Model for Separated Turbulent Flows," AIAA Paper 78-257, 1978.

6. Hung, C., and MacCormack, R., "Numerical Solution of Three-Dimensional Shock Wave and Turbulent Boundary Layer Interaction," AIAA J., Vol. 16, 1978, pp. 1090-1096.

7. Deiwert, G., "Numerical Simulation of Three-Dimensional Boattail Afterbody Flowfields," AIAA J., Vol. 19, 1981, pp. 582-588.

8. Hung, C. and Chaussee, D., "Computation of Supersonic Turbulent Flows Over an Inclined Ogive-Cylinder Flare," AIAA Paper 80-1410, 1980.

9. Pulliam, T. and Steger, J., "Implicit Finite-Difference Simulations of 3-D Compressible Flows," AIAA J., Vol. 18, 1980, pp. 159-167.

10. Horstman, C., Hung, C., Settles, G., Vas, I., and Bogdonoff, S., "Reynolds Number Effects on Shock-Wave Turbulent Boundary Layer Interaction - A Comparison of Numerical and Experimental Results," AIAA Paper 77-42, 1977.

11. Shang, J. and Hankey, W., "Numerical Solution for Supersonic Turbulent Flow Over a Compression Ramp," AIAA J., Vol. 13, 1975, pp. 1368-1374.

12. Settles, G., Bogdonoff, S., and Vas, I., "Incipient Separation of a Supersonic Turbulent Boundary Layer at High Reynolds Number," AIAA J., Vol. 14, 1976, pp. 50-56.

13. Settles, G., Fitzpatrick, T., and Bogdonoff, S., "Detailed Study of Attached and Separated Compression Corner Flowfields in High Reynolds Number Supersonic Flow," AIAA J., Vol. 17, 1979, pp. 579-585.

14. Settles, G., Gilbert, R., and Bogdonoff, S., "Data Compilation for Shock Wave/Turbulent Boundary Layer Interaction Experiments on Two-Dimensional Compression Corners," Report MAE-1489, Dept. of Mech. and Aero. Engr., Princeton University, 1980.

15. Rubesin, M. and Rose, W., "The Turbulent Mean-Flow, Reynolds-Stress, and Heat-Flux Equations in Mass-Averaged Dependent Variables," NASA TMX-62248, March 1973.

16. Visbal, M. and Knight, D., "Evaluation of the Baldwin-Lomax Turbulence Model for Two-Dimensional Shock Wave Turbulent Boundary Layer Interactions," AIAA Paper No. 83-1697, AIAA 16th Fluid and Plasma Dynamics Conference, July 12-14, 1983.

17. Visbal, M., "Numerical Simulation of Shock/Turbulent Boundary Layer Interactions Over 2-D Compression Corners," Ph.D. Thesis, Department of Mechanical and Aerospace Engineering, Rutgers University, New Brunswick, NJ, October 1983.

18. Cebeci, T. and Smith, A., Analysis of Turbulent Boundary Layers, Academic Press, New York, 1974.

19. Bradshaw, P., "Effects of Streamline Curvature on Turbulent Flow," AGARDograph No. 169, 1973.

20. Bradshaw, P., "The Effect of Mean Compression or Dilation on the Turbulence Structure of Supersonic Boundary Layers," J. Fluid Mech., Vol. 63, Part 3, 1974, pp. 449-464.

21. Beam, R. and Warming, R., "An Implicit Factored Scheme for the Compressible Navier-Stokes Equations," AIAA J., Vol. 16, 1978, pp. 393-402.

22. Sun, C.-C. and Childs, M., "Wall-Wake Velocity Profile for Compressible Nonadiabatic Flows," AIAA J., Vol. 14, 1976, pp. 820-822.

23. Visbal, M. and Knight, D., "Generation of Orthogonal and Nearly Orthogonal Coordinates with Grid Control Near Boundaries," AIAA J., Vol. 20, No. 3, 1982, pp. 305-306.

24. Knight, D., "Theoretical Investigation of Three-Dimensional Shock-Wave Turbulent Boundary Layer Interactions," Interim Report for Period 1 October 1981 to 30 September 1982, AFOSR Grant 82-0040, Report RU-TR-157-MAE-F, Department of Mechanical and Aerospace Engineering, Rutgers University, New Brunswick, New Jersey, December 1982; AFOSR TR-83-0230, 1983.

25. Delery, J., "Experimental Investigation of Turbulence Properties in Transonic Shock/Boundary-Layer Interactions," AIAA J., Vol. 21, No. 2, 1983, pp. 180-185.

26. Settles, G., Baca, B., Williams, D., and Bogdonoff, S., "A Study of Reattachment of a Free Shear Layer in Compressible Turbulent Flow," AIAA Paper No. 80-1408, 1980.

27. McCabe, A., "The Three-Dimensional Interaction of a Shock Wave with a Turbulent Boundary Layer," The Aeronautical Quarterly, Vol. 17, 1966, pp. 231-252.

28. Law, C., "Three-Dimensional Shock Wave-Turbulent Boundary Layer Interactions at Mach 6," Aero. Res. Labs., ARL-TR-75-0191, Wright-Patterson AFB, OH, June 1975.

29. Peake, D., "Three Dimensional Swept Shock/Turbulent Boundary Layer Separations with Control by Air Injection," Aero. Report LR-592, National Research Council-Canada, July 1976.

30. Oskam, B., Vas, I., and Bogdonoff, S., "Mach 3 Oblique Shock Wave/ Turbulent Boundary Layer Interactions in Three Dimensions," AIAA Paper 76-336, 1976.

31. Oskam, B., Vas, I., and Bogdonoff, S., "An Experimental Study of Three-Dimensional Flow Fields in an Axial Corner at Mach 3," AIAA Paper 77-689, 1977.

32. Oskam, B., Vas, I., and Bogdonoff, S., "Oblique Shock Wave/Turbulent Boundary Layer Interactions at Mach 3," AFFDL-TR-76-48, Part I (1976), Part II (1978), Air Force Flight Dynamics Laboratory, Wright-Patterson AFB, Ohio.

33. Kubota, H. and Stollery, J., "An Experimental Study of the Interaction Between a Glancing Shock Wave and a Turbulent Boundary Layer," J. Fluid Mech., Vol. 116, 1982, pp. 431-458.

34. McClure, W., "An Experimental Study into the Scaling of an Unswept Sharp-Fin-Generated Shock/Turbulent Boundary Layer Interaction," M.S.E. Thesis, Department of Mechanical and Aerospace Engineering, Princeton University, January 1983.

35. McClure, W. and Dolling, D., "Flowfield Scaling in Sharp Fin-Induced Shock Wave Turbulent Boundary Layer Interaction," AIAA Paper No. 83-1754, 1983.

36. Buleev, N., "Theoretical Model of the Mechanism of Turbulent Exchange in Fluid Flows," AERE Translation 957, Atomic Energy Research Establishment, Hartwell, England, 1963.

37. Gessner, F. and Po, J., "A Reynolds Stress for Turbulent Corner Flows - Part II: Comparisons Between Theory and Experiment," J. Fluids Engr., Trans. of ASME, Vol. 98, Series I, No. 2, pp. 269-277, 1976.

38. Knight, D., "A Hybrid Explicit-Implicit Numerical Algorithm for the Three-Dimensional Compressible Navier-Stokes Equations," AIAA Paper 83-0223, January 1983.

39. Knight, D., "Improved Calculation of High Speed Inlet Flows. Part I: Numerical Algorithm," AIAA J., Vol. 19, 1981, pp. 34-41.

40. Deiwert, G., "Numerical Simulation of High Reynolds Number Transonic Flows," AIAA J., Vol. 13, 1975, pp. 1354-1359.

41. Rakich, J., Vigneron, Y., and Tannehill, J., "Navier-Stokes Calculations for Laminar and Turbulent Hypersonic Flow Over Indented Nosetips," AIAA Paper 78-260, 1978.

42. MacCormack, R., "Numerical Solution of the Interaction of a Shock Wave with a Laminar Boundary Layer," Lecture Notes in Physics, Vol. 8, 1971 pp. 151-163.

43. Baldwin, B. and MacCormack, R., "A Numerical Method for Solving the Navier-Stokes Equations with Application to Shock-Boundary Layer Interactions," AIAA Paper No. 75-1, 1975.

44. Keller, H., "Accurate Difference Methods for Nonlinear Two-Point Boundary Value Problems," SIAM J. Numerical Analysis, Vol. 11, 1974, pp. 305-320.

45. Knight, D., "Improved Calculation of High Speed Inlet Flows. Part II: Results," AIAA J., Vol. 19, 1981, pp. 172-179.

46. Knight, D., "Calculation of High-Speed Inlet Flows Using the Navier-Stokes Equations," J. Aircraft, Vol. 18, 1981, pp. 748-754.

47. Knight, D., "Calculation of a Simulated 3-D High Speed Inlet Using the Navier-Stokes Equations," AIAA Paper No. 83-1165, 1983.

48. Smith, R. and Pitts, J., "The Solution of the Three-Dimensional Viscous-Compressible Navier-Stokes Equations on a Vector Computer," Advances in Computer Methods for Partial Differential Equations - Proc. of the Third IMACS Symposium, 1979, pp. 245-252.

49. Lambiotte, J., "Effect of Virtual Memory on Efficient Solution of Two Model Problems," NASA TMX 3512, 1977.

50. Knight, J., "SL/1 Manual," Analysis and Computation Division, Programming Techniques Branch, NASA Langley Research Center, June 1979; Revised October 1981.

51. CDC CYBER 203 Fortran Language (Version) 1.4 Reference Manual, Control Data Corporation, Publication No. 60457040, July 1979, CDC Publications and Graphics Division, Sunnyvale, California.

52. CDC CYBER 203 Fortran Language (Version) 2.0 Reference Manual, Control Data Corporation, Publication No. 60485000, CDC Publications and Graphics Division, Sunnyvale, California.

53. Settles, G., Perkins, J., and Bogdonoff, S., "Investigation of Three-Dimensional Shock/Boundary Layer Interactions at Swept Compression Corners," AIAA J., Vol. 18, 1980, pp. 779-785.

54. Settles, G., Perkins, J., and Bogdonoff, S., "Upstream Influence Scaling of 2-D and 3-D Shock/Turbulent Boundary Layer Interactions at Compression Corners," AIAA Paper No. 81-0334, 1981.

55. Teng, H. and Settles, G., "Cylindrical and Conical Upstream Influence Regimes of 3-D Shock/Turbulent Boundary Layer Interactions," AIAA Paper No. 82-0987, 1982.

END

DATE
FILMED

4 84

DTIC